THE ASTROPHYSICAL JOURNAL SUPPLEMENT SERIES, 99:297–348, 1995 August

THE FIRST CALTECH–JODRELL BANK VLBI SURVEY. III. VLBI AND MERLIN OBSERVATIONS AT 5 GHz AND VLA OBSERVATIONS AT 1.4 GHz

W. XU, A. C. S. READHEAD, AND T. J. PEARSON
Owens Valley Radio Observatory, California Institute of Technology, Pasadena, CA 91125

AND

A. G. POLATIDIS AND P. N. WILKINSON
University of Manchester, Nuffield Radio Astronomy Laboratories, Jodrell Bank, Macclesfield, Cheshire SK11 9DL, England, UK
Received 1994 November 28; accepted 1995 January 26

ABSTRACT

We present the 5 GHz results from the first Caltech–Jodrell Bank (CJ1) VLBI survey. The 1.6 GHz maps were presented in two separate papers (Polatidis et al. 1995; Thakkar et al. 1995). These three papers complete the first stage of this program to map at both 1.6 and 5 GHz all objects accessible to Mark II VLBI in the complete sample of 135 objects with $1.3 > S_{5\,\mathrm{GHz}} \geq 0.7$ Jy, $\delta(1950) \geq 35°$, and $|b| > 10°$. The combination of the CJ1 sample with the Pearson-Readhead (PR) sample provides a complete, flux density–limited sample of 200 objects with $S_{5\,\mathrm{GHz}} \geq 0.7$ Jy, $\delta(1950) \geq 35°$, and $|b| > 10°$ for which all of the objects accessible to Mark II VLBI have been mapped at both 5 GHz (129 objects) and 1.6 GHz (132 objects).

In addition to the 5 GHz VLBI maps, we present in this paper 5 GHz MERLIN observations of 20 objects and 1.4 GHz VLA observations of 92 objects in the combined CJ1 + PR sample. The VLA maps, together with *L*-band (1.3–1.7 GHz) maps available in the literature, provide a complete set of VLA maps for the combined CJ1 + PR sample. Finally, we present the radio spectra of the objects in the CJ1 sample.

The combined CJ1 + PR VLBI surveys provide a sample which is large enough for a number of important astrophysical and cosmological studies. These will be presented in further papers in this series.

Subject headings: quasars: general — radio continuum: galaxies — surveys

1. INTRODUCTION

This is the third paper in a series presenting results of the first Caltech–Jodrell Bank VLBI survey (the CJ1 Survey). The CJ1 sample comprises the 135 objects from the S4 and S5 surveys (Pauliny-Toth et al. 1978; Kühr et al. 1981a) with 1.3 Jy $> S_{5\,\mathrm{GHz}} \geq 0.7$ Jy, $\delta(1950) \geq 35°$, and $|b| \geq 10°$. Together with the Pearson-Readhead sample (Pearson & Readhead 1988, hereafter PR) of objects with $S_{5\,\mathrm{GHz}} \geq 1.3$ Jy, the CJ1 + PR sample has a combined total of 200 objects with $S_{5\,\mathrm{GHz}} \geq 0.7$ Jy, $\delta(1950) \geq 35°$, and $|b| \geq 10°$.

Some of the objects in the sample do not contain a bright, compact component and thus are not suitable for imaging with the global Mark II VLBI network. As described in Paper I (Polatidis et al. 1995), we used previous VLBI and VLA observations to exclude unsuitable sources, that is, sources that were known to contain no component smaller than 2″ and stronger than 300 mJy at centimeter wavelengths. We did include some sources with weaker compact cores when there was prior evidence of milliarcsecond-scale structure.

In Papers I and II (Polatidis et al. 1995; Thakkar et al. 1995) we cataloged the sample and presented the results of 1.6 GHz VLBI observations of 81 objects in the CJ1 sample accessible to Mark II VLBI imaging and 31 objects from the PR sample that had not previously been imaged with VLBI at 1.6 GHz. In this paper we present the 5 GHz VLBI observations of the 87 objects in the CJ1 sample and the one remaining object in the PR sample accessible to Mark II VLBI. These three papers, combined with the 5 GHz maps of PR and maps available in the literature, provide a complete set of VLBI maps at 1.6 and 5 GHz of all objects accessible to Mark II VLBI in the CJ1+PR sample.

In addition to the 5 GHz VLBI maps of CJ1 objects, we present radio spectra of all CJ1 objects, 1.4 GHz VLA maps of 92 objects, and five GHz MERLIN maps of 20 objects from the combined CJ1+PR sample. The objects mapped with the VLA are those CJ1+PR objects for which no adequate VLA maps exist in the literature. Thus, the VLA maps presented here, plus those available in the literature, provide an almost uniform set of ~1.4 GHz maps of the large-scale radio structure of the complete CJ1+PR sample.

The VLBI maps presented in these three papers were made with the "snapshot" technique, which has proved extremely effective in mapping compact structure in radio sources and increases the efficiency of VLBI arrays by over a factor ~20. The technique is described in detail by Polatidis et al. (1995).

The results of the combined CJ1+PR surveys provide a sample which is large enough for a number of important astrophysical and cosmological studies—including determination of physically distinct classes, proper motion–redshift tests, angular diameter–redshift tests, and misalignment between parsec-scale and kiloparsec-scale radio structures. In particular, there were some classes of object in the PR sample with very few members, and these have now been augmented significantly by the addition of the CJ1 objects. The dual-wavelength observations presented in these three papers provide for a much more secure classification of radio-loud active galaxies than do single-frequency observations. The classification of these objects

will be discussed in a later paper in this series. In addition, a number of interesting objects—including compact symmetric objects and possible gravitational lenses—have been discovered in the course of the 1.6 and 5 GHz VLBI surveys. These topics will be addressed in a number of papers describing follow-up studies of the CJ1 survey.

2. OBSERVATIONS AND DATA REDUCTION

2.1. *VLBI Observations and Data Reduction*

We observed 87 objects in the CJ1 sample with the global VLBI network at 5 GHz. Observations were recorded with left circular polarization (IEEE convention) and with a bandwidth of 1.8 MHz, using the Mark II VLBI format (Clark 1973), and cross-correlated with the JPL/Caltech Block 2 correlator. One object, 0404+768, in the PR sample was also observed since it had not been mapped previously at 5 GHz. All objects, except 0218+357 and 0404+768, were observed with the snapshot technique (Polatidis et al. 1995)—generally with three 20–30 minute scans, but a few objects had one or two extra scans; 0218+357 was observed for 4.5 hr and 0404+768 for 3 hr. The observations were completed in six sessions between 1990 and 1992 (Table 1). Thirteen to 17 stations participated in each session. The locations and parameters of the stations are listed in Table 1. In the session of 1991 September we obtained simultaneous MERLIN observations. Data from three of the six MERLIN stations (Cambridge, Mark II at Jodrell Bank, and Knockin) were recorded in Mark II format for cross-correlation with the non-MERLIN stations. The MERLIN data were combined with VLBI data, giving 21 stations in this session. The length of the snapshots was shortened from 30 minutes to 20 minutes during the course of this project as we gained confidence in the technique. To optimize the *uv* coverage, the three snapshots were scheduled as follows: for objects with mutual observing time of 8 hr or longer, the snapshots were separated by about 4 hr, which provided very good *uv* coverage; for other objects, three snapshots were taken at the beginning, the middle, and the end of the mutual observing time. For objects with a declination near 35°, the lower limit of our sample, the mutual observing time is only ~4 hr, which leaves large holes in the *uv* coverage and may lead to uncertainties in the map. In these cases one or two stations were often given up in order to gain ~1.5 hr or more in mutual observing time. Figure 1 shows the *uv* coverage for three representative objects, at $\delta \simeq 38°$, $\delta \simeq 52°$, and $\delta \simeq 77°$.

After correlation, data were fringe-fitted with the NRAO Astronomical Image Processing System (AIPS) program FRING (1994 July edition), the global fringe-fitting algorithm developed by Schwab & Cotton (1983). Nyquist search windows, i.e., 2000 ns in delay and 500 mHz in rate centered on zero, were used. The Effelsberg 100 m antenna was chosen as the reference antenna whenever possible; otherwise, the Green Bank 140 foot (43 m) telescope was selected. The solution interval was set to 4–6 minutes in most cases, but values up to 15 minutes were used for weak objects. For 0218+357, a 2 minute interval was used since this object is a large double of separation ~330 mas. After fringe-fitting, the 2 s data were phase–self-calibrated in DIFMAP (Shepherd, Pearson, & Taylor 1994) with a 10 s solution time to remove the residual phase errors. A point source model was used for all objects except 0218+357, for which a model with two Gaussian components, derived from EVN observations (A. R. Patnaik, private communication), was used. The data were then averaged coherently for 60 s in all but two cases. An averaging interval of 10 s was used for 0218+357 and 30 s for 0404+768 to avoid significant time-average smearing. The error bars of the averaged data were calculated from the scatter of individual data points within the averaging period.

Amplitude calibration was performed with the program CAL in the Caltech VLBI package, which calibrates the correlation coefficients using measurements of antenna system temperatures and antenna gain curves (Cohen et al. 1975). Station-dependent calibration gain factors were derived from the observations of the strong, barely resolved, or highly core-dominated calibrator objects 0133+476, 0552+398, 1638+398, and 1739+522. These gain factors were applied to the entire observing session. We believe that the final calibration is good to ~5%. Time-dependent calibration errors were later corrected by self-calibration. After calibration, the data were edited in DIFMAP.

All of the objects were first mapped and self-calibrated noninteractively using an automatic script, called AUTOMAP, to drive DIFMAP. In AUTOMAP the data are first phase–self-calibrated with a point source model, and then a "dirty" image is produced by Fourier inversion. The position of the highest surface brightness feature on the dirty map is then identified, and a small rectangular window is centered on this position. The map is then "CLEANed" (Högbom 1974) for a number of iterations, with a loop gain of typically ~0.01. In each CLEAN iteration the highest surface brightness feature remaining within the window in the residual or "difference" map is subtracted from the data. AUTOMAP then performs another phase self-calibration using the clean-component model and makes a new difference map. It finds the position of the highest surface brightness feature in this map, adds another window centered on this position, and repeats the above process. In later loops amplitude self-calibration is allowed in addition to phase self-calibration. After some experimentation we developed a final version of AUTOMAP in which (1) the CLEAN loop had a cutoff at 6 σ, where σ is the residual rms noise in the difference map; (2) a Gaussian taper with a value of 0.3 at a spacing of 50 Mλ in the *uv* plane was applied to the visibility amplitudes—this helped to show up any faint extended structure; and (3) amplitude self-calibration was applied, followed by more CLEAN loops with a cutoff at 4.5 σ. Note that the rms noise on the residual map was changing during the above process, so the CLEAN cutoff was adjusted for each step. After choosing adequate map sizes, ~60% of the maps generated by AUTOMAP are equivalent to those made interactively, and ~35% contain slight errors at low levels and can be corrected interactively with ease. The rest had to be mapped interactively with care. Even for these objects, the structure revealed by AUTOMAP is basically correct. AUTOMAP failed entirely on only one—complex—object, 1311+678.

Our final procedure generated three images: a uniformly weighted map, a naturally weighted map, and a map made from data which had been tapered with a Gaussian function with a value 0.3 at 50 Mλ. The tapered maps have map sizes 4 times as large as the others to search for structure on larger scales. The final maps are limited by thermal noise in most

TABLE 1

TELESCOPE CHARACTERISTICS

Telescope	Code	Location	Diameter (meter)	Sensitivity (K/Jy)	T_{sys} (K)	Network	1990 Mar	1991 Jun	1991 Sep	1992 Mar	1992 Jun	1992 Sep
Onsala	S	Sweden	26	0.059	150	EVN	√	√	√	√	√	√
Effelsberg	B	Germany	100	2.38	45	EVN	√	√	√		√	√
WSRT	W	Netherlands	14×25	—[a]	110	EVN	√	√	√	√	√	√
JBNK	J2	Jodrell Bank, UK	25	0.12	46	EVN, MERLIN		√	√	√		
Medicina	L	Bologna, Italy	32	0.16	45	EVN	√	√	√	√	√	√
Noto	No	Noto, Italy	32	0.146	45	EVN	√	√	√	√	√	√
Cambridge	C	Cambridge, UK	32	0.23	32	MERLIN			√	√		
Knockin	Kn	Knockin, UK	25	0.12	33	MERLIN			√			
Tabley	T	Tabley, UK	25	0.13	34	MERLIN			√			
Defford	De	Defford, UK	25	0.032	55	MERLIN			√			
Darnhall	Da	Darnhall, UK	25	0.12	32	MERLIN			√			
Haystack	K	Westford, MA, USA	36	0.16	74	US	√	√	√	√	√	√
NRAO	G	Green Bank, WV, USA	43	0.27	33	US	√	√	√	√	√	√
FDVS	F	Fort Davis, TX, USA	26	0.095	88	US	√					
VLBA_Nl	Nl	North Liberty, IA, USA	25	0.142	40	VLBA		√	√	√	√	√
VLBA_Fd	Fd	Fort Davis, TX, USA	25	0.131	42	VLBA		√	√	√	√	√
VLBA_La	La	Los Alamos, NM, USA	25	0.139	40	VLBA	√	√	√	√	√	√
VLBA_Pt	Pt	Pie Town, NM, USA	25	0.126	42	VLBA	√	√	√	√	√	√
VLBA_Kp	Kp	Kitt Peak, AZ, USA	25	0.128	43	VLBA	√	√	√	√	√	√
VLBA_Ov	Ov	Owens Valley, CA, USA	25	0.124	36	VLBA				√	√	√
VLBA_Br	Br	Brewster, WA, USA	25	0.130	34	VLBA			√	√	√	√
VLA[b]	Y	Socorro, NM, USA	25	0.119	37	US	√	√	√	√	√	√
OVRO	O	Owens Valley, CA, USA	40	0.201	70	US	√	√	√			

[a] WSRT provided T_{sys} in K and Jy, from which the sensitivity could be derived. The value varied from 0.3 to 1, depending on the number of antennas actually used.

[b] The VLA was used in single-antenna mode.

NOTES.—Cols. (1)–(3): The name, code, and location of each telescope. Col. (4): The diameter of each telescope (in meters). Cols. (5)–(6): The sensitivity in kelvins per jansky and system temperature in kelvins of each telescope. Col. (7): The network with which each telescope is associated. Cols. (8)–(13): A tick indicates whether the telescope participated in that session.

AFFILIATIONS.—O, Onsala Space Observatory; B, Max-Planck-Institute für Radiostronomie; W, Westerbork Synthesis Radio Telescope; J2, MK II telescope, Nuffield Radio Astronomy Laboratories; L, No, Instituto di Radioastronomia; C, Kn, T, De, Da, Nuffield Radio Astronomy Laboratories; K, Haystack Observatory; G, National Radio Astronomy Observatory; F, George A. Agassiz Station of Harvard University; Nl, Fd, La, Pt, Kp, Ov, Br, National Radio Astronomy Observatory, VLBA; Y, National Radio Astronomy Observatory, VLA; O, Owens Valley Radio Observatory.

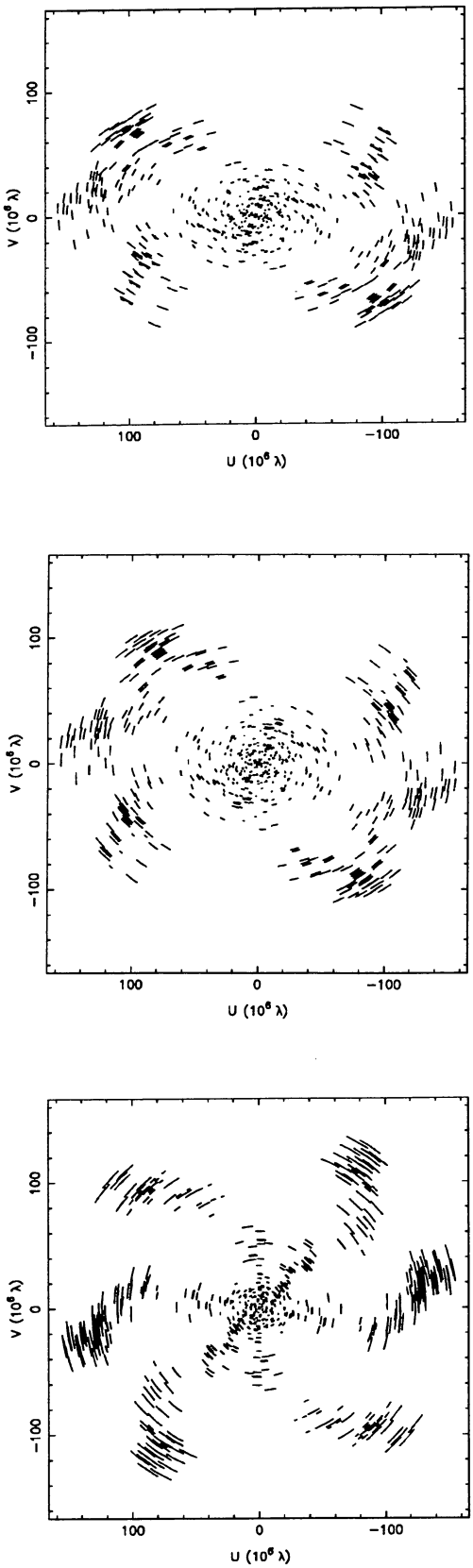

FIG. 1.—Typical *uv* coverages for VLBI observations. *Top:* $\delta \simeq 38°$ (1438+385 observed on 1992 June 6); *middle:* $\delta \simeq 52°$ (1317+520 observed on 1992 June 6); *bottom:* $\delta \simeq 77°$ (1357+769 observed on 1991 June 8).

cases. The typical rms noise in a blank area in the map is ~0.5 mJy with natural weighting and ~1 mJy with uniform weighting. The dynamic range of the images (i.e., the ratio of the brightest feature in the map to rms noise in a blank area) is larger than 300:1 in most cases. Four objects, 0707+689, 0827+378, 1203+645, and 1637+626, were very heavily resolved and detected on only a few short baselines and were not mapped. The naturally weighted and tapered maps of the other 84 objects are presented in Figure 2. The objects 0218+357, 0821+394, 1138+594, and 1437+624 have large angular sizes, and we present maps of individual components so that more detail can be seen. The parameters of the maps are listed in Table 2.

The final step in the data analysis was to fit the closure phases and self-calibrated amplitudes with elliptical Gaussian models using the program MODELFIT in the Caltech VLBI package (Pearson 1991). Such models provide a parameterization of the object structure, which is useful both for comparing structural changes between epochs and for estimating physical parameters. The models and agreement factors (square root of reduced χ^2) between the models and observed visibilities are listed in Table 3. Separate agreement factors are given for amplitude and closure phase. In addition a "total" agreement factor (a weighted average of the amplitude and closure phase agreement factors) is given; this is the quantity that is minimized in the least-squares model-fitting procedure. A detailed description of the agreement factor is given by Henstock et al. (1995).

In addition to the 87 CJ1 objects discussed in this paper, six other CJ1 objects have been observed with global VLBI or the EVN at 1.6 GHz (Paper I and references therein). A good quality 5 GHz map of 1637+826 (NGC 6251) has been published by Jones et al. (1986); thus, we did not observe it. The objects 0010+775, 0945+664, and 2324+405 were heavily resolved at 1.6 GHz, while 1250+568 and 2323+435 have no bright compact feature in their 1.6 GHz EVN images and hence are not accessible to Mark II VLBI observations. Therefore, we did not attempt to observe these five objects at 5 GHz.

2.2. *MERLIN Observations and Data Reduction*

MERLIN observations at 5 GHz of 20 objects in the CJ1 and PR samples were made in 1992 February. Parameters for the MERLIN telescopes are summarized in Table 1. The object list is given in Table 4. Each object was observed with many 20–30 minute scans spanning ~12 hr, with a total integration time from 4 to 6 hr. Our observations were made with left circular polarization (IEEE convention) and recorded with a bandwidth of 7 MHz separated into seven 1 MHz channels. The data were calibrated with the OLAF package of the Nuffield Radio Astronomy Laboratories. The objects 3C 286 and OQ 208 were used as the flux density calibrators. Bandpass corrections were made with the AIPS package. The maps were made with DIFMAP. Typical *uv* coverages are shown in Figure 3. Uniformly weighted maps are presented in Figure 4. For four objects with large-scale structure, naturally weighted maps restored with a circular Gaussian beam of FWHM 100 mas are also presented. For the object 0812+367 we include a map of the central and southern component to show more detail. Its northern component is slightly resolved. The parameters of the maps are listed in Table 4.

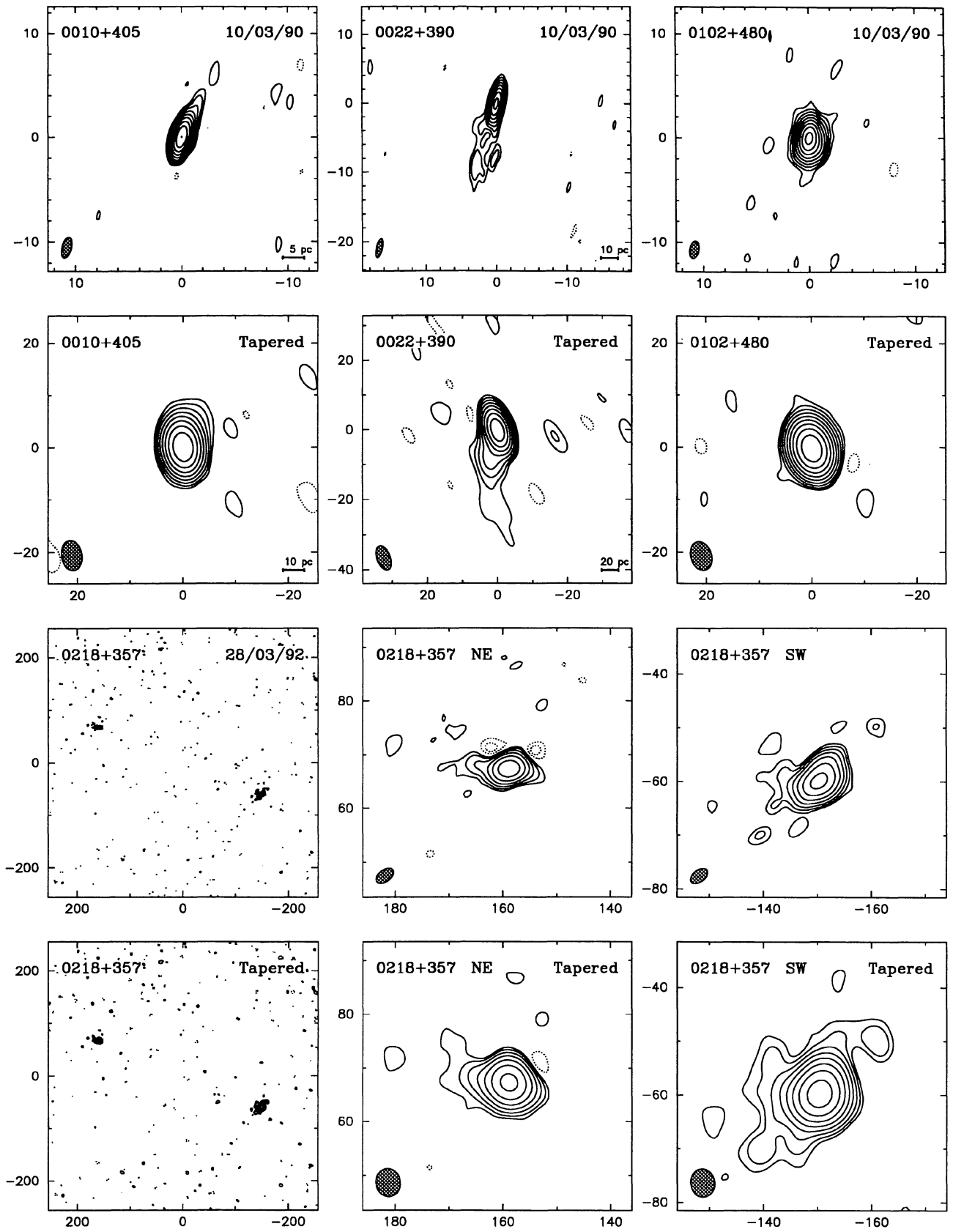

FIG. 2.—The 5 GHz VLBI maps of 84 objects. For each object the upper panel shows the naturally weighted map, and the lower panel shows the tapered map. Logarithmic contour levels are used in all maps, at $-2, -1, 1, 2, 4, 8, 16, \cdots 1024 \times 3\ \sigma$ (where σ is the rms noise measured in a blank region of the map). The objects 0218+357, 0821+394, 1138+594, and 1437+624 have large angular sizes, and maps of individual components are also presented. The FWHM contour of the elliptical Gaussian restoring beam is shown hatched in the lower left-hand corner. The peak intensity, rms noise, and parameters of the restoring beam are listed in Table 3. The angular scale is marked in milliarcseconds, and, where the redshift is known, the linear scale of each map is indicated in the lower right-hand corner (assuming $H_0 = 100$ km s^{-1} Mpc^{-1} and $q_0 = 0.5$). FITS images corresponding to the maps presented in Fig. 2 are published in the AAS CD-ROM Series, Vol. 5.

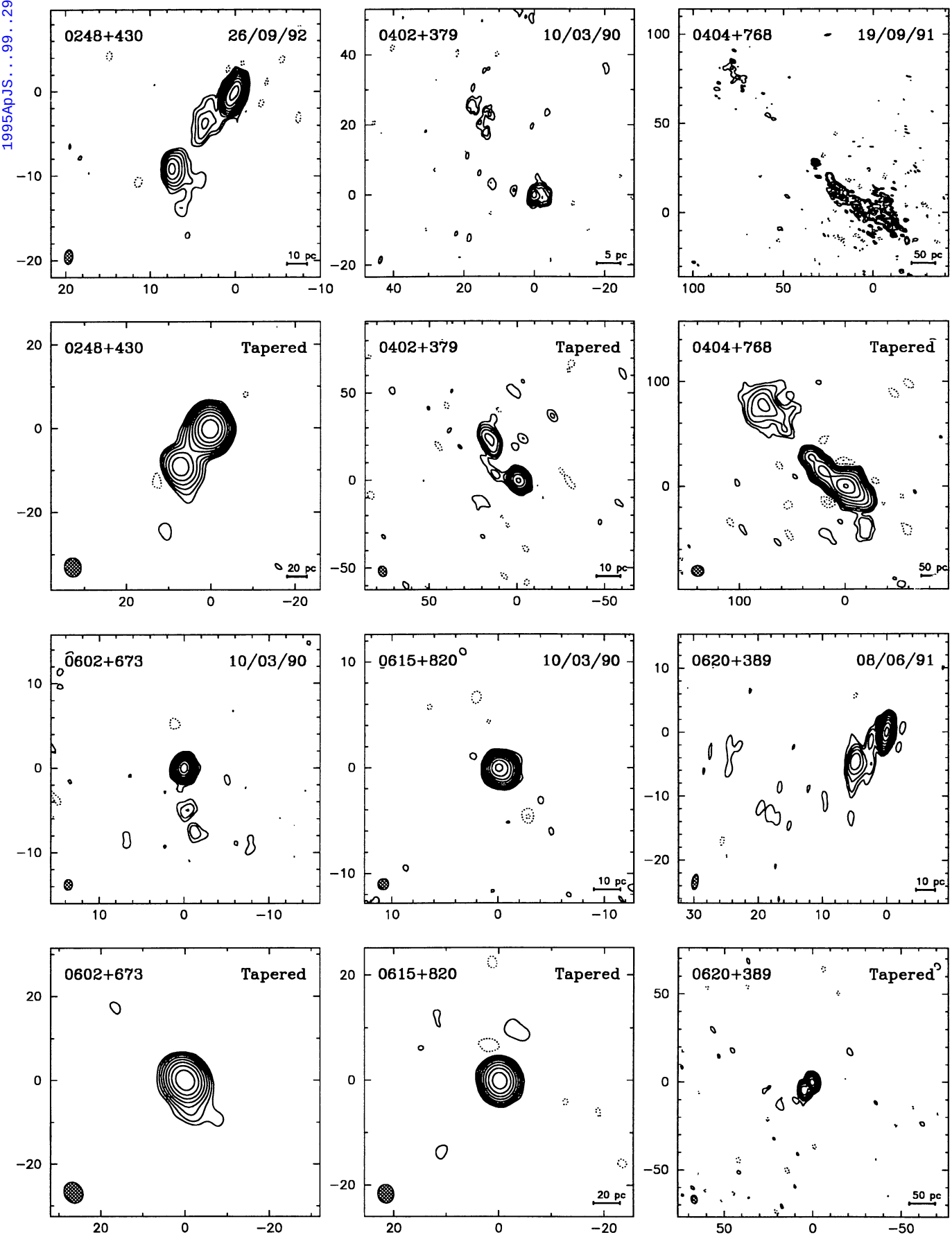

FIG. 2—*Continued*

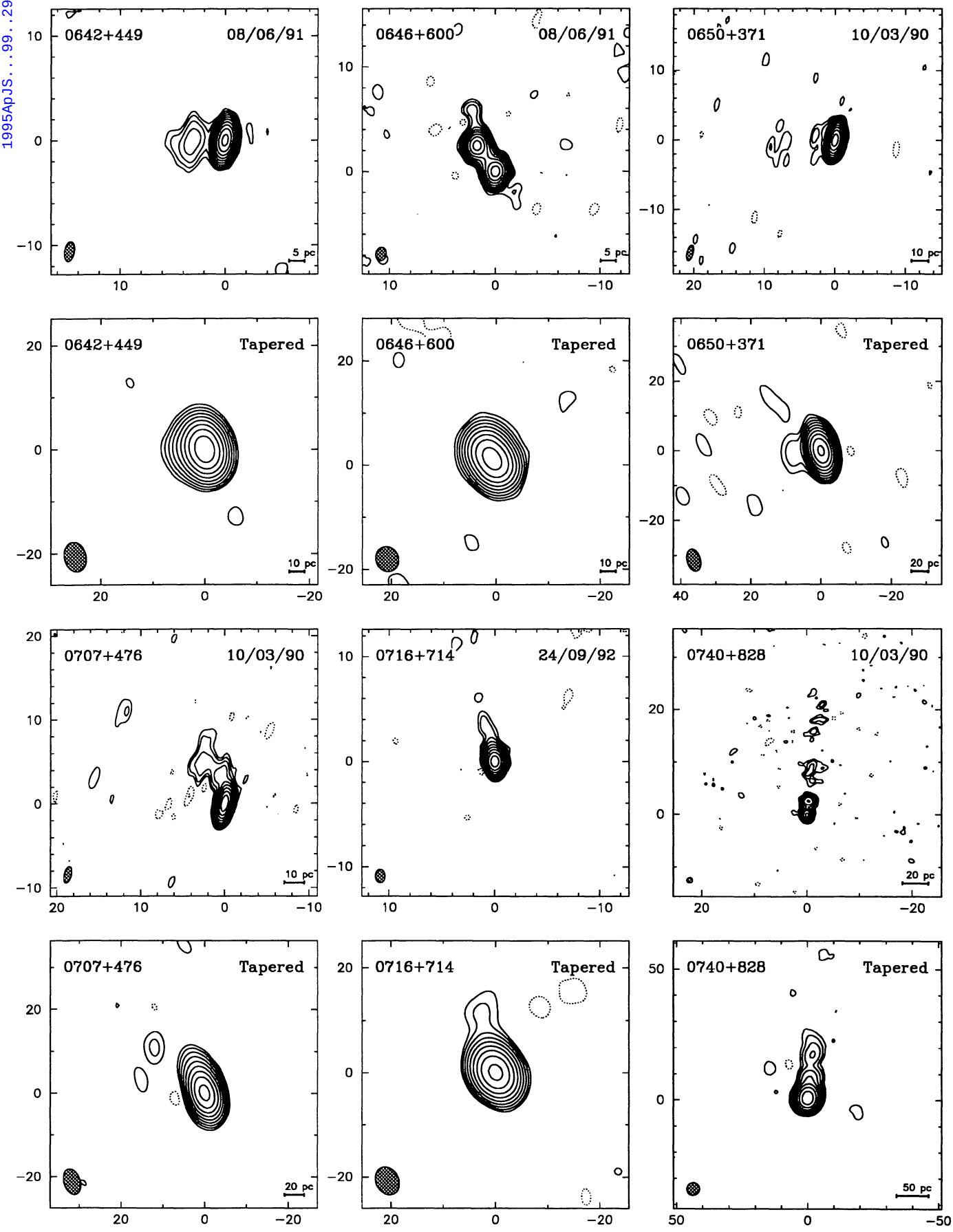

FIG. 2—*Continued*

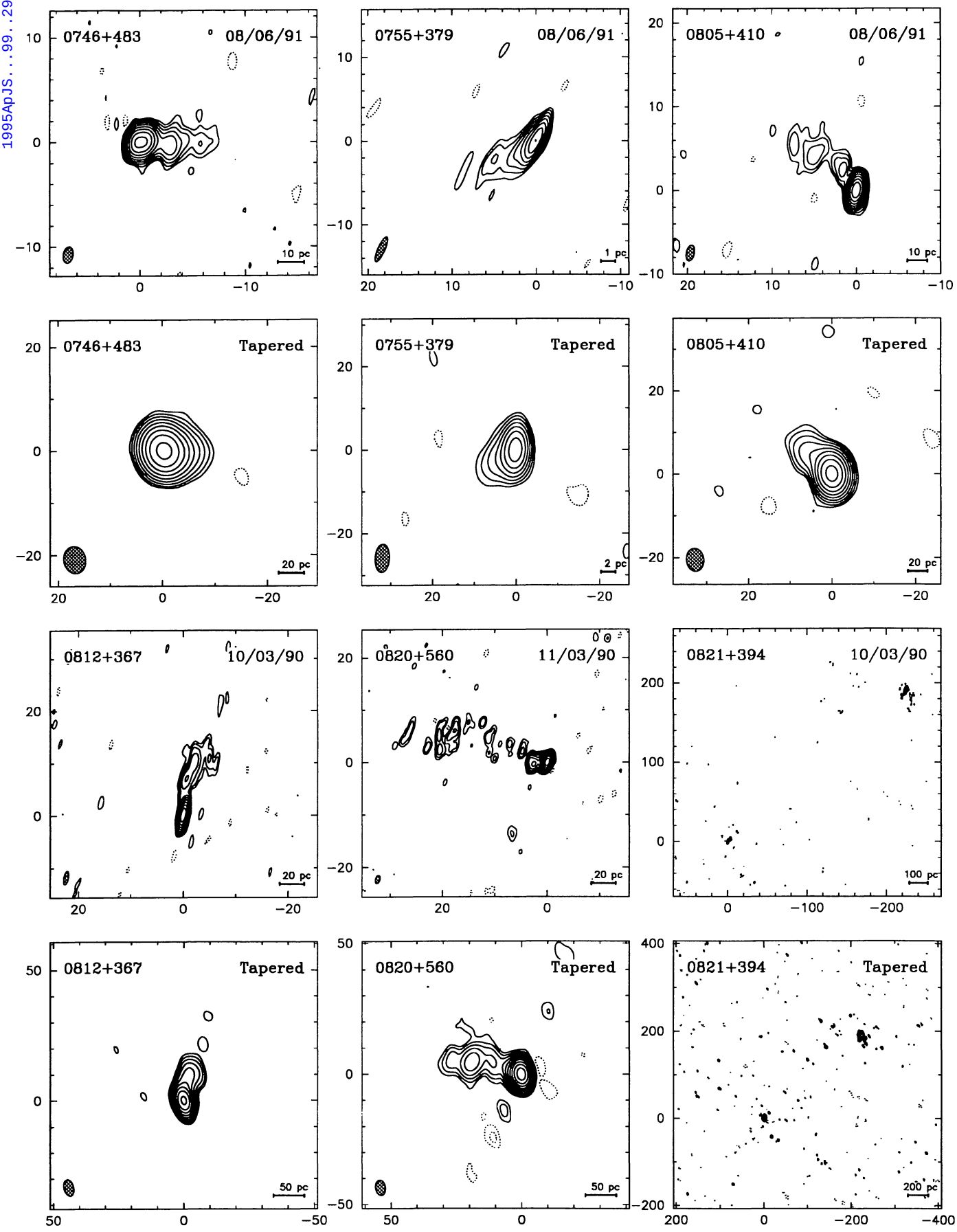

FIG. 2—*Continued*

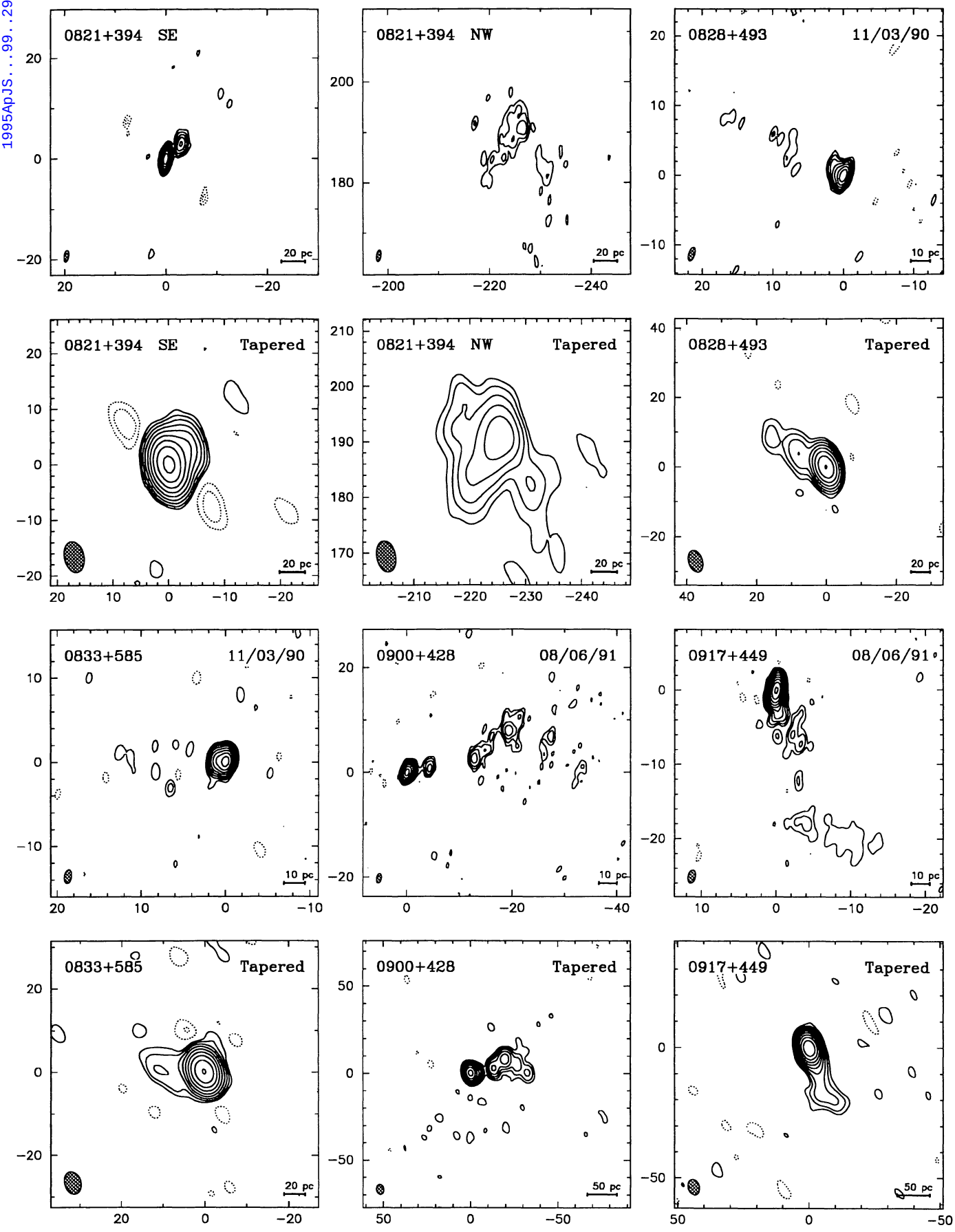

FIG. 2—*Continued*

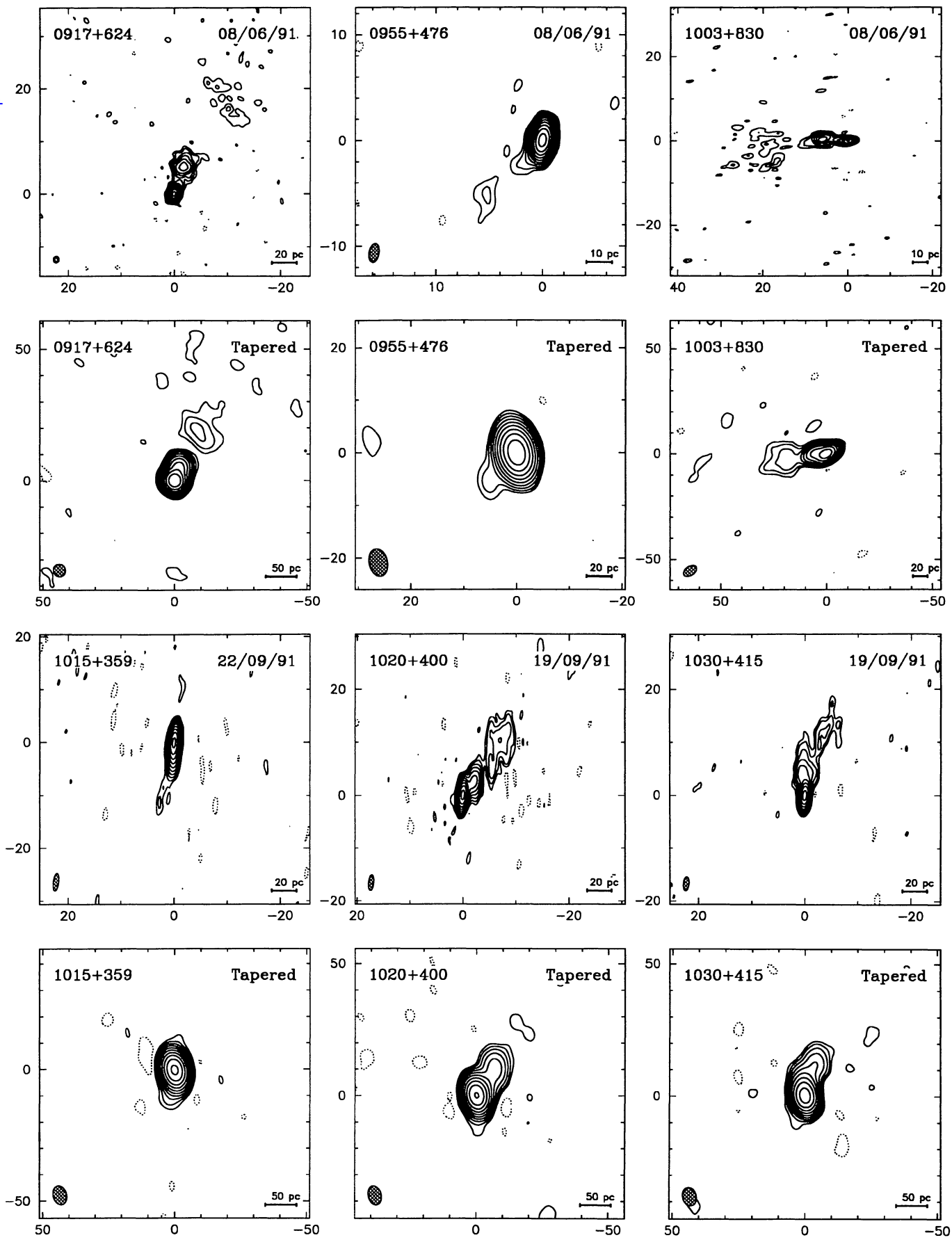

FIG. 2—*Continued*

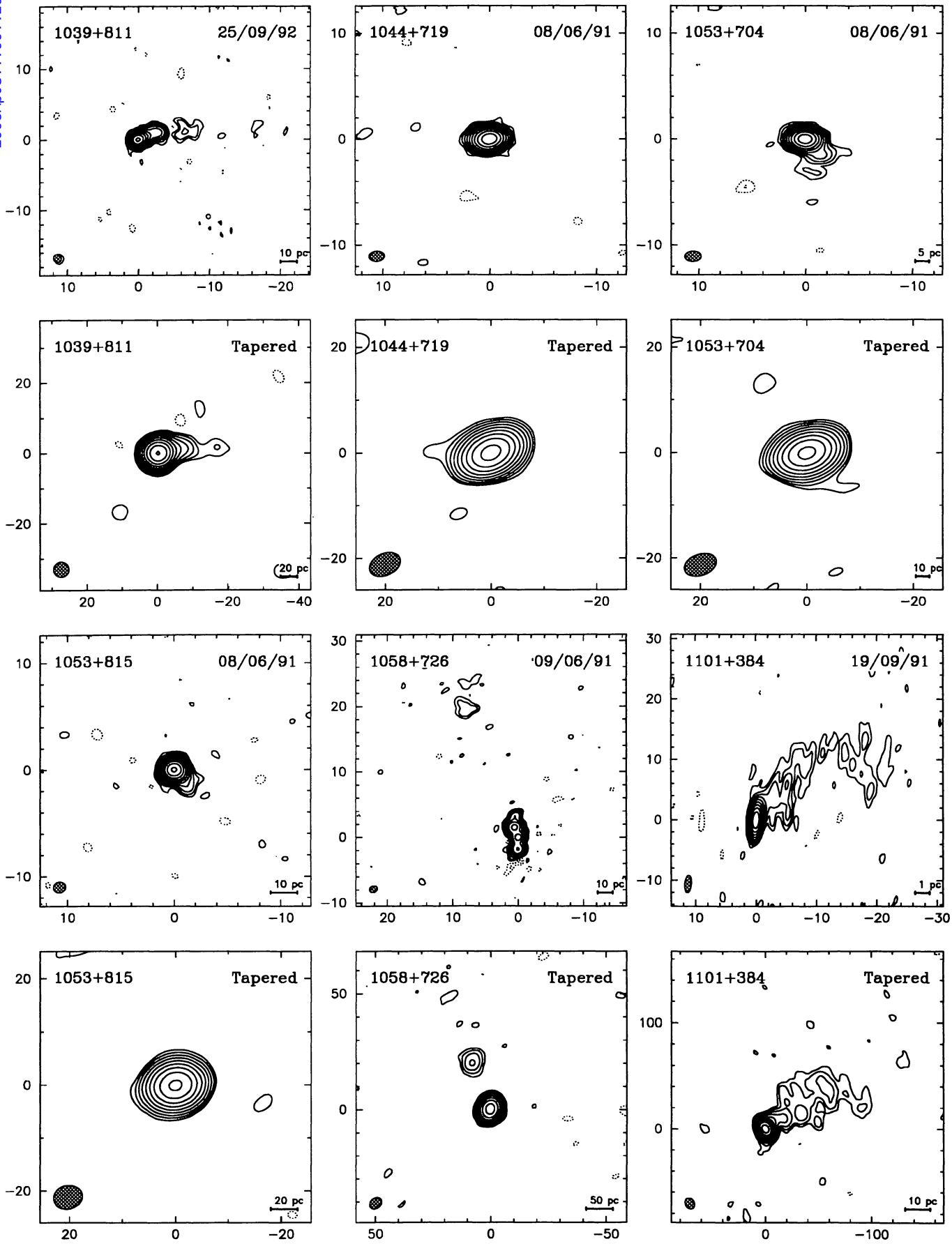

FIG. 2—*Continued*

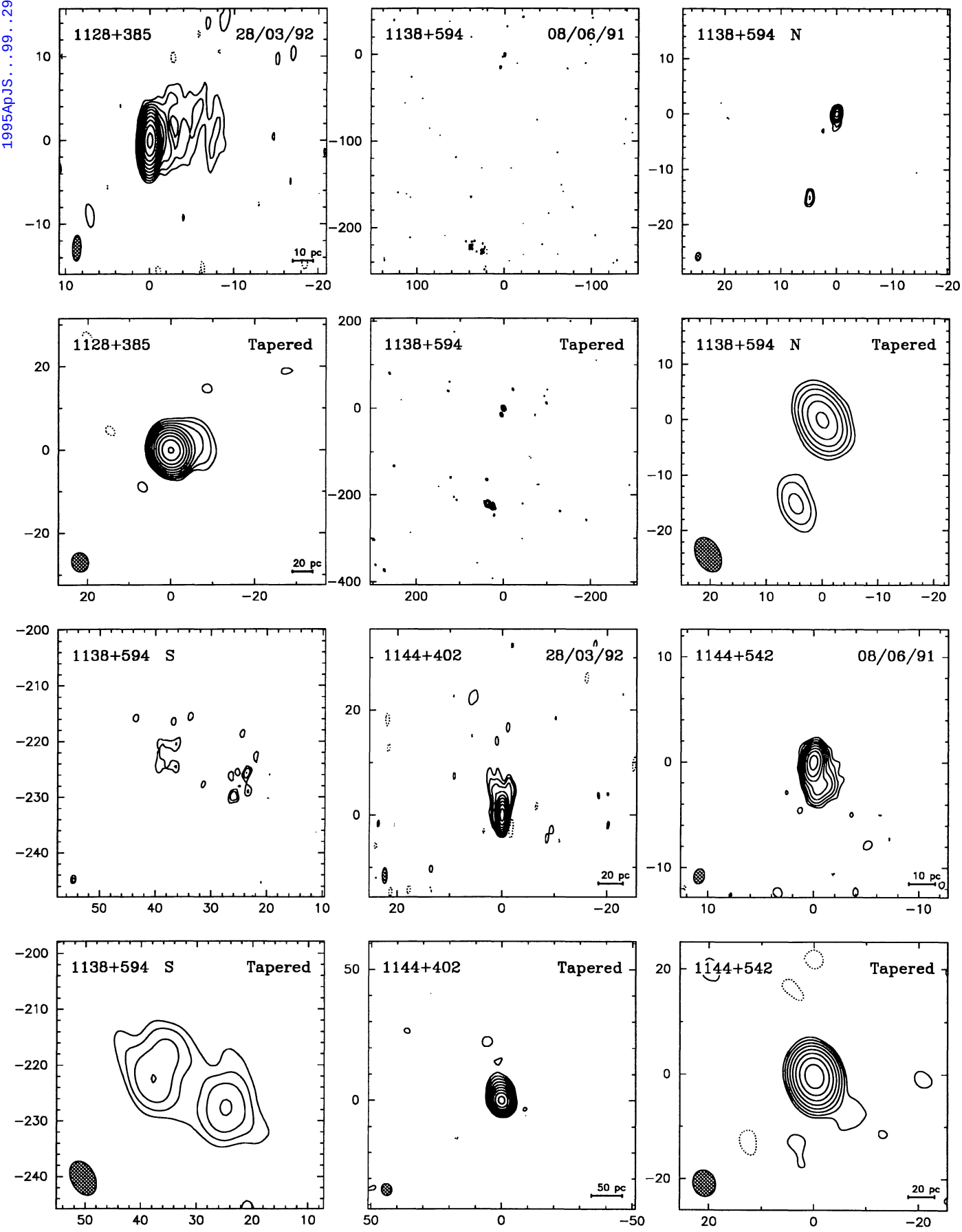

FIG. 2—*Continued*

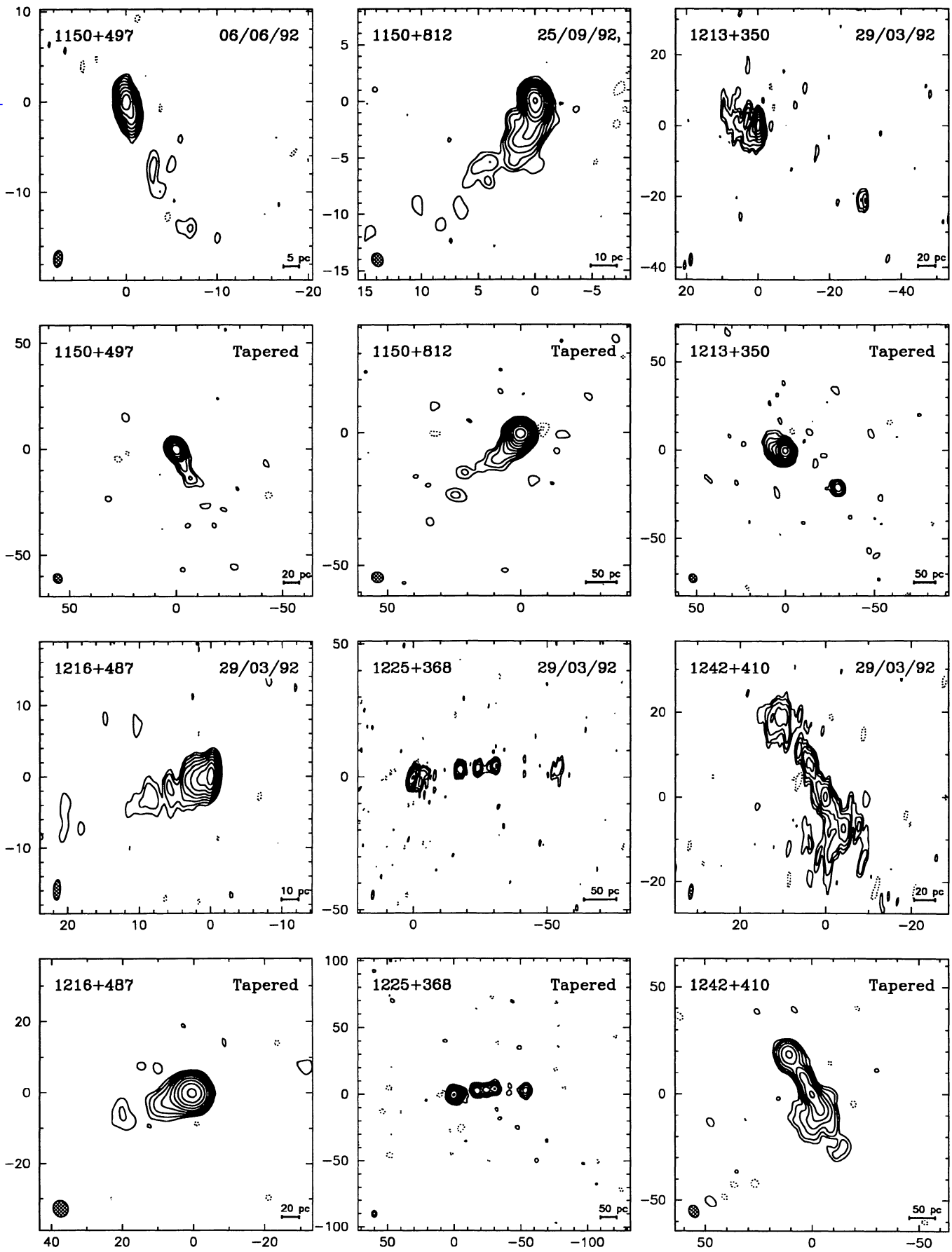

FIG. 2—*Continued*

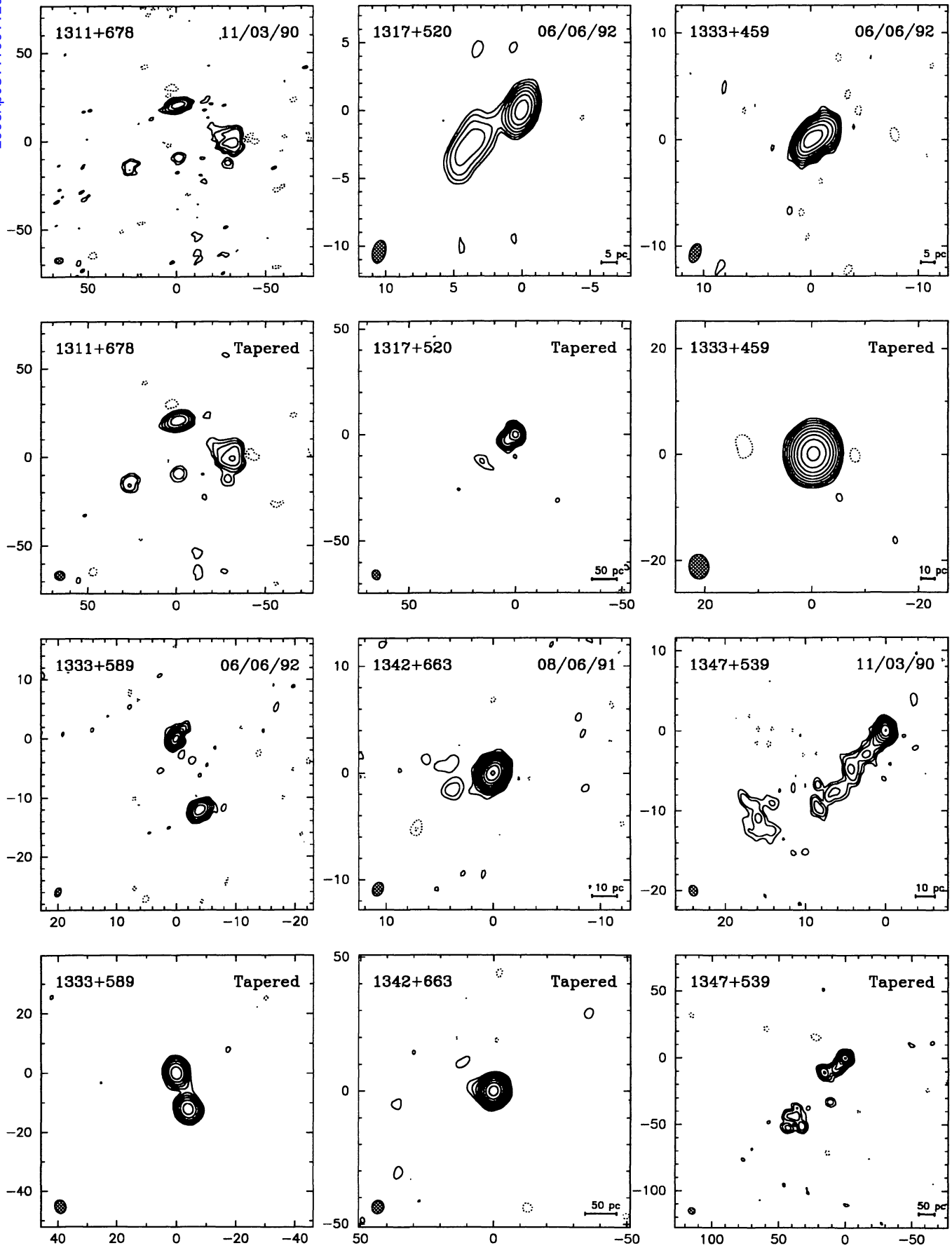

FIG. 2—*Continued*

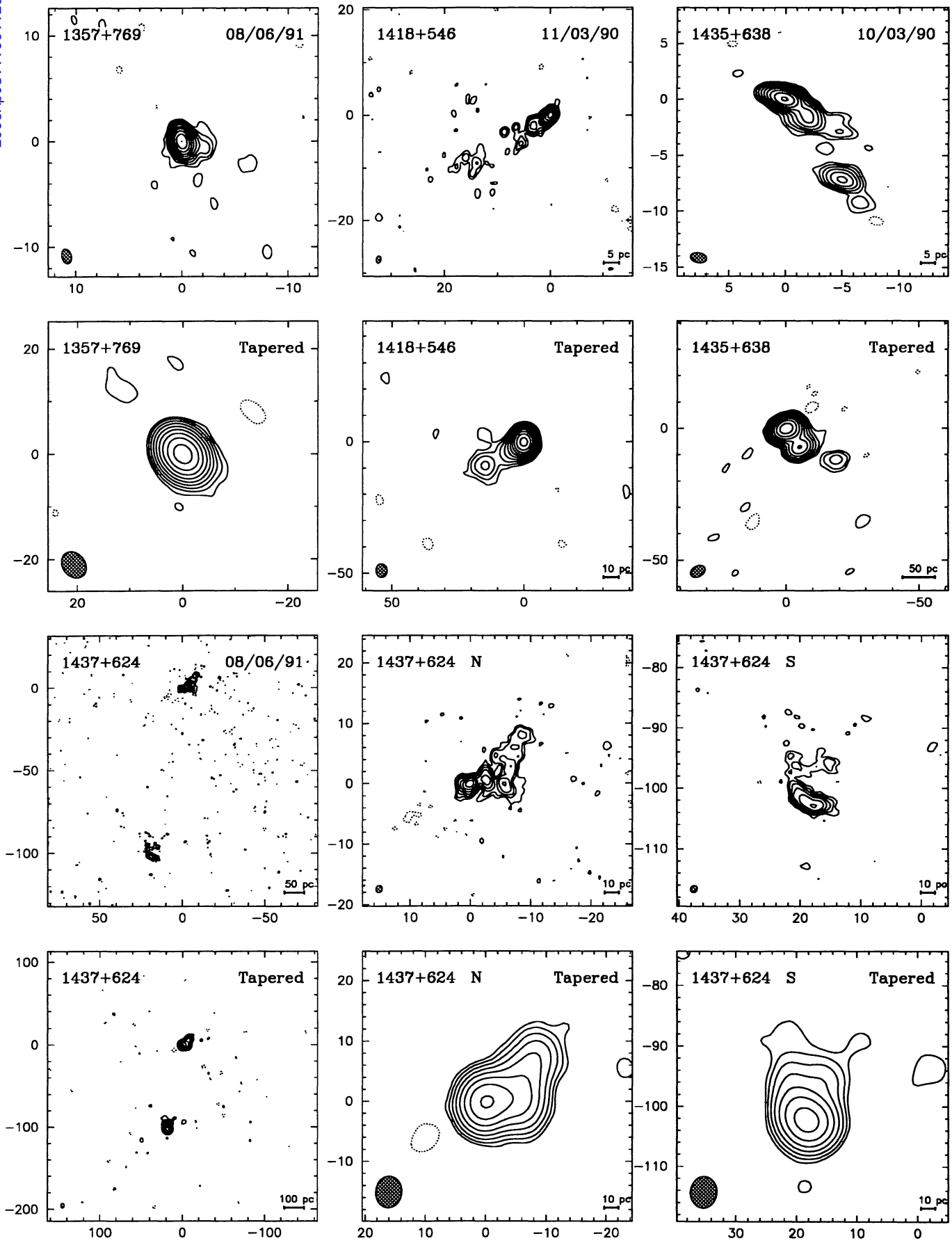

FIG. 2—*Continued*

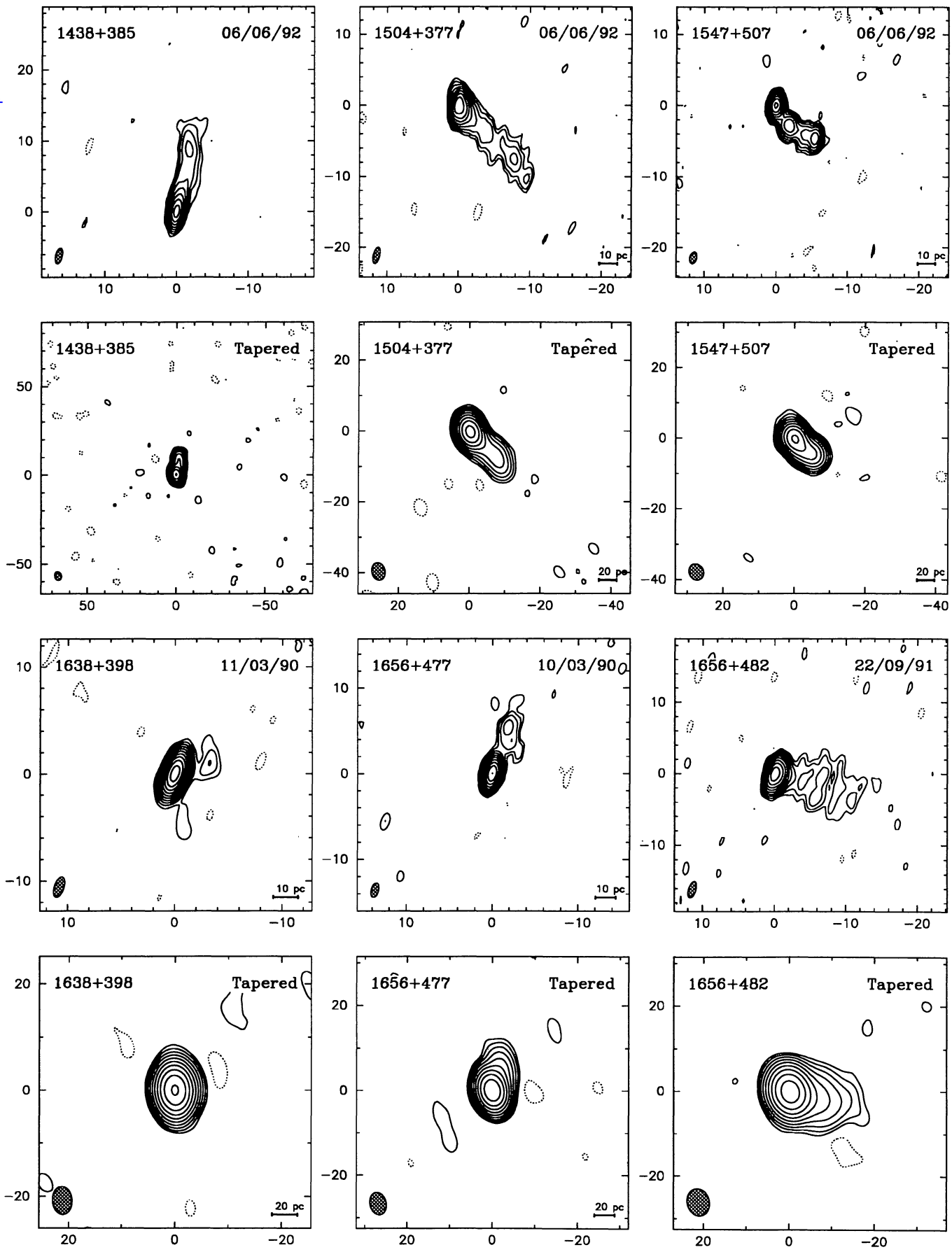

FIG. 2—*Continued*

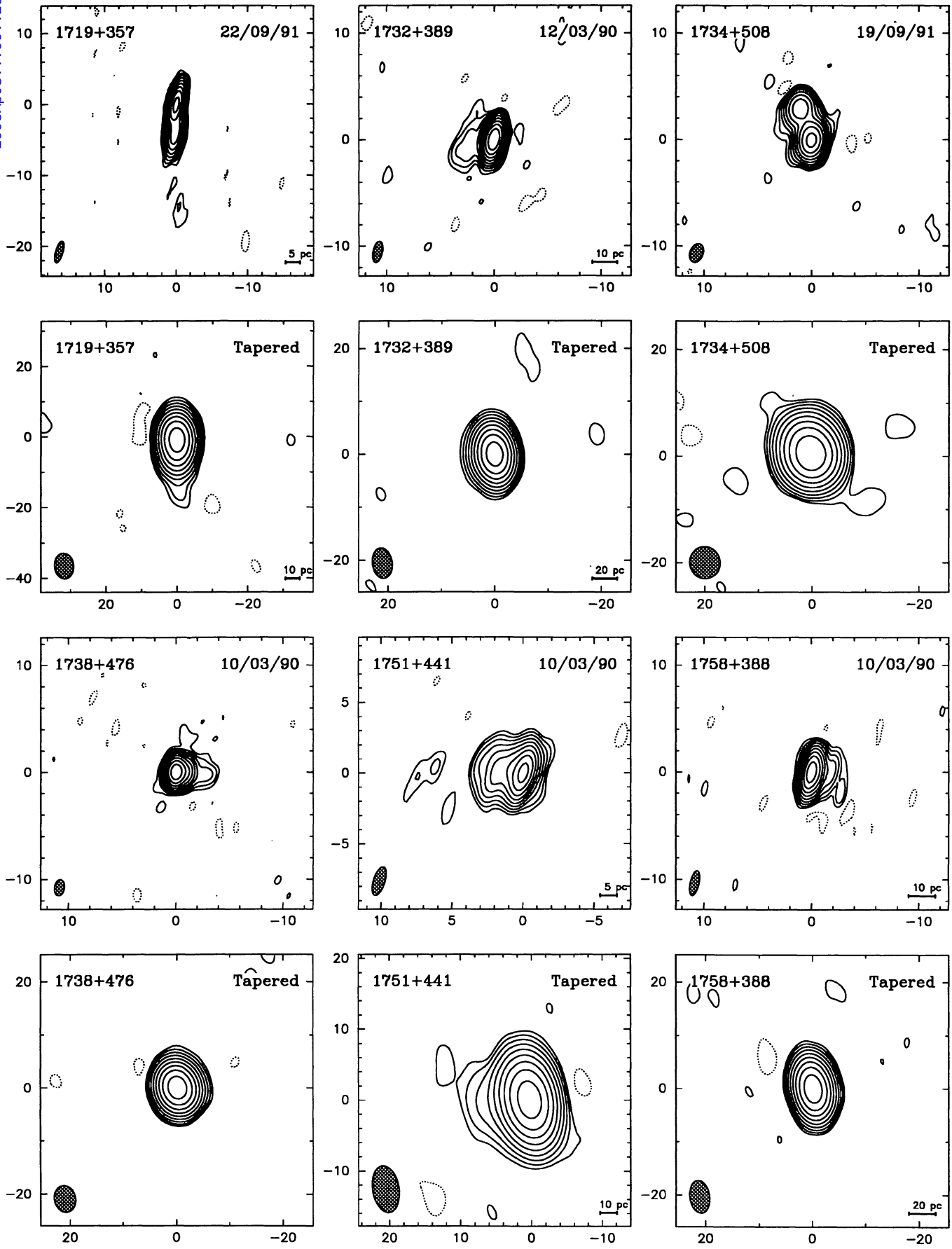

FIG. 2—*Continued*

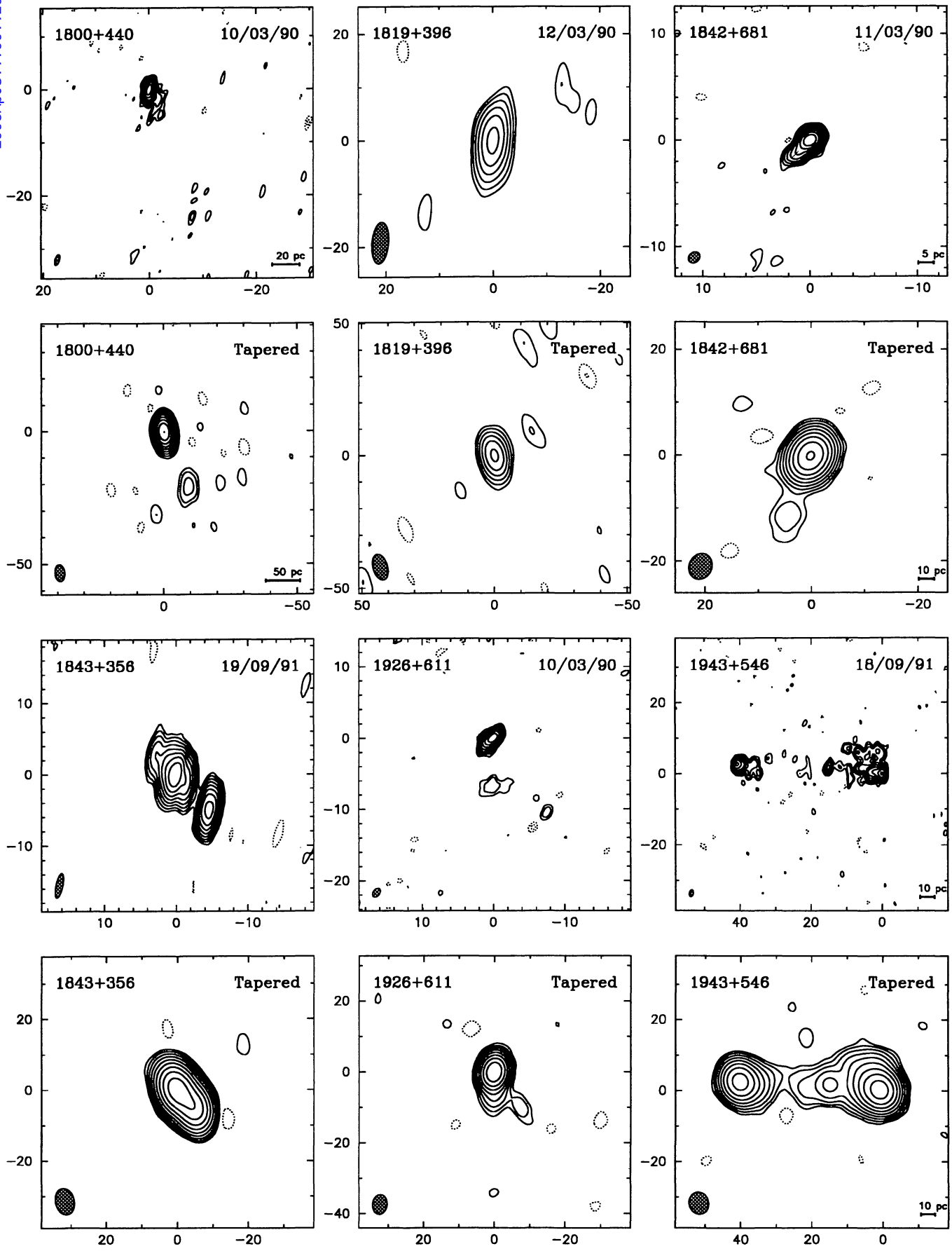

FIG. 2—*Continued*

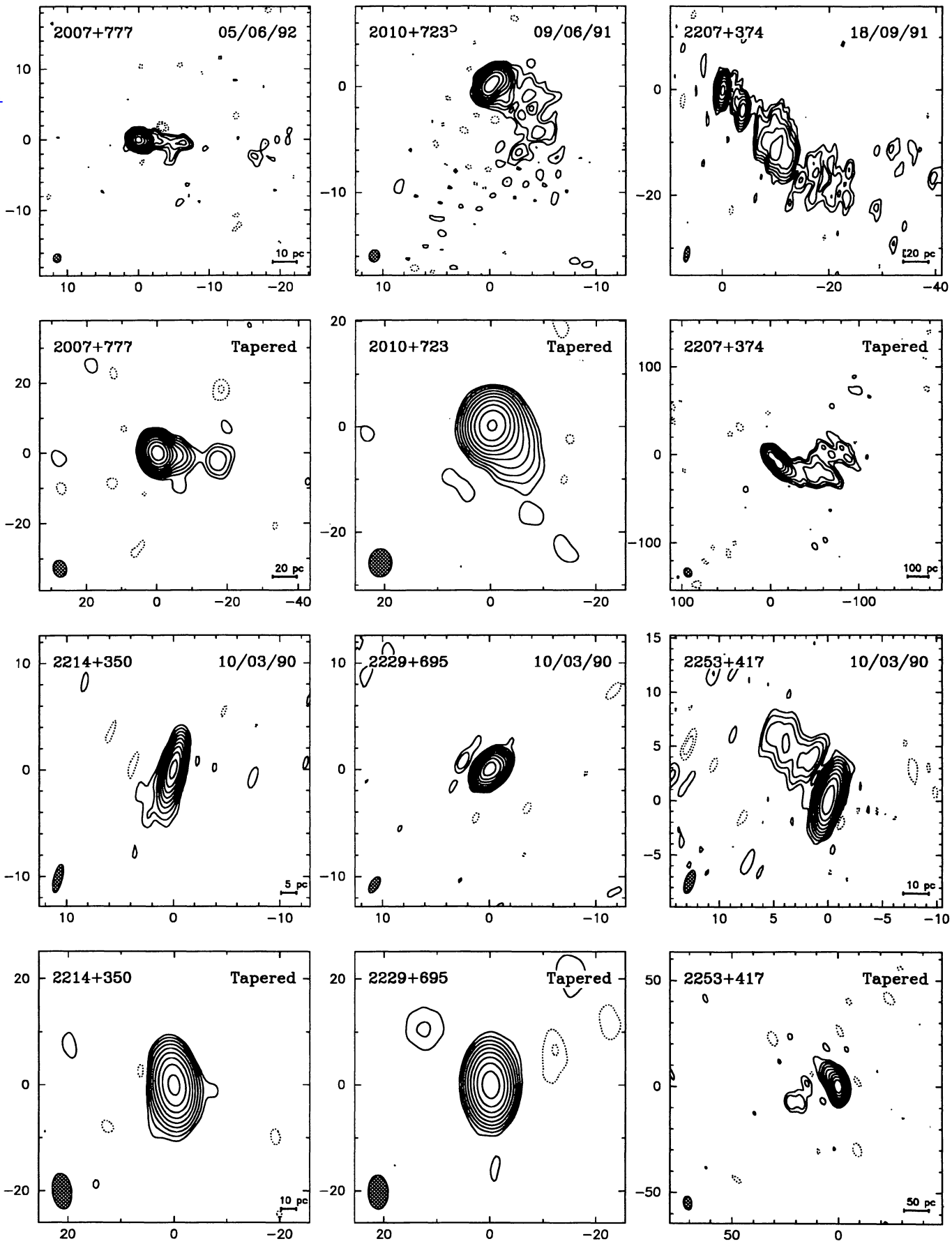

FIG. 2—*Continued*

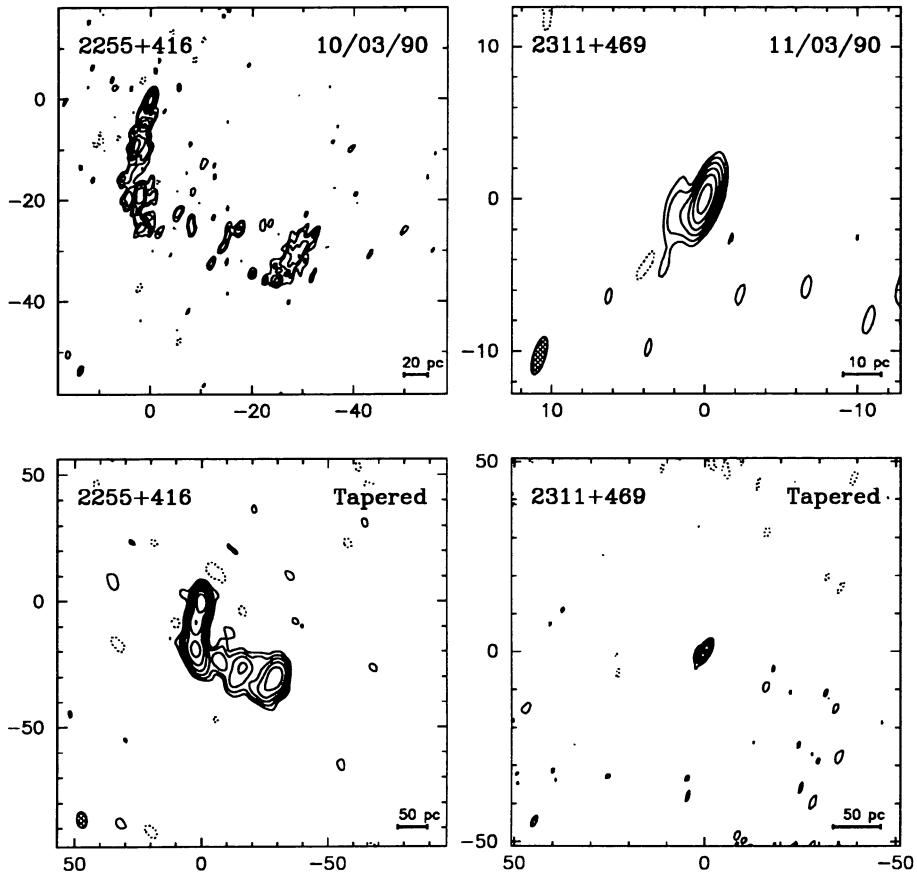

FIG. 2—*Continued*

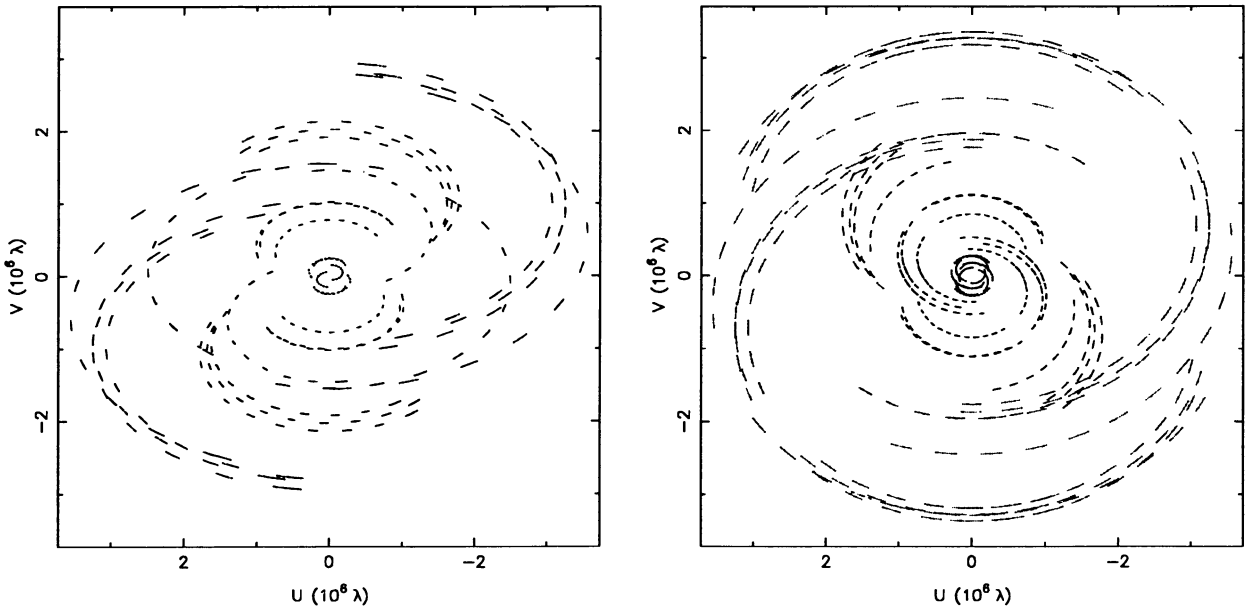

FIG. 3.—Typical *uv* coverages for MERLIN observations. *Left:* $\delta \simeq 37°$ (0812+367 observed on 1992 February 4); *right*: $\delta \simeq 54°$ (1347+539 observed on 1992 February 6).

TABLE 2

VLBI MAP PARAMETERS

Source	Observation	NATURALLY WEIGHTED MAPS					TAPERED MAPS				
		Beam[a]			S_{peak}	rms	Beam			S_{peak}	rms
		a (mas)	b (mas)	θ (°)			a (mas)	b (mas)	θ (°)		
0010+405	1990 Mar	2.0	0.9	−14	417.0	0.5	5.8	3.9	10	466.0	0.6
0022+390	1990 Mar	2.7	0.8	−12	395.0	0.8	7.3	3.8	20	518.0	0.8
0102+480	1990 Mar	1.7	0.9	−11	695.0	0.7	5.6	3.9	18	1060.0	0.8
0218+357[c]	1992 Mar	3.7	2.2	−52	221.3	0.7	5.2	4.5	6	380.0	0.7
0248+430	1992 Sep	1.7	1.0	−7	609.0	0.6	4.5	4.0	12	982.0	0.7
0402+379	1990 Mar	2.1	0.9	−17	143.0	1.0	6.0	4.6	22	413.0	0.9
0404+768	1991 Sep	1.9	1.2	70	153.0	1.0	11.4	10.1	84	997.6	1.2
0602+673	1990 Mar	1.2	1.0	−7	560.0	0.4	5.2	4.3	30	649.0	0.9
0615+820	1990 Mar	1.1	1.0	−29	458.0	0.5	3.6	3.1	9	717.0	1.1
0620+389	1991 Jun	2.4	0.9	−9	403.0	0.4	4.8	3.2	12	464.0	0.8
0642+449	1991 Jun	1.9	0.9	−10	1470.0	0.7	5.8	4.2	14	1580.0	1.2
0646+600	1991 Jun	1.3	1.0	−11	430.0	0.4	4.9	4.3	24	813.0	0.7
0650+371	1990 Mar	2.3	0.8	−14	959.0	0.4	6.5	3.8	14	1280.0	0.7
0707+476	1990 Mar	2.0	0.8	−14	645.0	0.5	6.3	3.8	18	770.0	0.8
0707+689[b]	1991 Jun										
0716+714	1992 Sep	1.3	0.9	1	598.0	0.5	5.6	4.4	28	640.0	0.7
0740+828	1990 Mar	1.1	1.0	−82	310.0	0.6	5.0	4.7	−44	573.0	0.9
0746+483	1991 Jun	1.6	1.0	−11	439.0	0.4	5.2	4.3	13	757.0	0.8
0755+379	1991 Jun	3.2	0.8	−24	143.0	0.4	6.8	3.5	−4	175.0	0.6
0805+410	1991 Jun	1.9	0.9	−12	910.0	0.6	5.5	4.1	7	966.0	0.9
0812+367	1990 Mar	2.6	0.8	−11	701.0	0.5	6.4	3.7	15	782.0	0.9
0820+560	1990 Mar	1.6	0.9	−17	1160.0	0.5	5.9	3.9	10	1320.0	0.6
0821+394[c]	1990 Mar	2.3	0.8	−9	642.0	0.9	5.6	3.5	12	694.0	0.7
0827+378[b]	1991 Jun										
0828+493	1990 Mar	2.0	0.8	−18	192.0	0.6	6.4	4.0	17	265.0	0.7
0833+585	1990 Mar	1.6	0.9	−10	386.0	0.7	5.5	3.9	19	604.0	0.8
0900+428	1991 Jun	1.8	0.9	−12	218.0	0.4	5.8	4.2	14	273.0	0.6
0917+449	1991 Jun	1.8	0.9	−12	973.0	0.6	6.0	4.2	17	1260.0	0.8
0917+624	1991 Jun	1.2	1.1	−8	843.0	0.4	4.9	4.6	28	1020.0	0.7
0955+476	1991 Jun	1.8	1.0	−10	993.0	0.5	5.3	3.5	14	1050.0	0.8
1003+830	1991 Jun	1.9	0.8	−81	258.0	0.3	6.9	4.1	−55	304.0	0.5
1015+359	1991 Sep	3.3	1.0	−7	569.0	0.3	7.3	5.1	15	668.0	0.4
1020+400	1991 Sep	3.0	1.0	−6	698.0	0.4	7.3	4.9	15	762.0	0.5
1030+415	1991 Sep	2.7	1.0	−6	282.0	0.3	6.9	5.1	16	324.0	0.3
1039+811	1992 Sep	1.1	1.1	61	869.0	0.5	4.4	4.3	−85	1090.0	0.7
1044+719	1991 Jun	1.5	0.9	−86	757.0	0.6	6.2	4.1	−65	958.0	0.9
1053+704	1991 Jun	1.6	0.9	−89	480.0	0.4	6.3	4.0	−70	556.0	0.6
1053+815	1991 Jun	1.2	1.0	−80	492.0	0.3	5.5	4.4	−77	554.0	0.6
1058+726	1991 Jun	1.3	1.0	−70	105.0	0.4	5.7	4.4	−54	311.0	0.6
1101+384	1991 Sep	2.9	1.1	−5	374.0	0.3	10.8	8.0	30	421.0	0.4
1128+385	1992 Mar	3.1	1.0	−3	823.0	0.4	4.6	4.0	14	936.0	0.6
1138+594[c]	1991 Jun	1.5	0.9	−9	79.2	0.6	6.6	4.2	27	90.0	0.8
1144+402	1992 Mar	3.0	1.0	−1	532.0	0.5	4.6	4.0	17	580.0	0.6
1144+542	1991 Jun	1.4	1.0	−14	230.0	0.4	5.1	4.2	14	349.0	0.6
1150+497	1992 Jun	1.8	0.9	−8	325.0	0.5	4.6	3.8	31	440.0	0.6

TABLE 2—*Continued*

Source	Observation	Naturally Weighted Maps					Tapered Maps				
		Beam[a]			S_{peak}	rms	Beam			S_{peak}	rms
		a (mas)	b (mas)	θ (°)			a (mas)	b (mas)	θ (°)		
1150+812	1992 Sep	1.2	1.0	25	727.0	0.4	4.6	3.9	79	1050.0	0.5
1203+645[b]	1990 Mar										
1213+350	1992 Mar	3.5	0.9	−3	433.0	0.7	4.9	4.2	18	691.0	0.7
1216+487	1992 Mar	2.9	1.0	−4	312.0	0.5	4.8	4.2	22	498.0	0.5
1225+368	1992 Mar	3.4	1.0	−6	226.0	0.6	4.8	4.1	8	457.0	0.6
1242+410	1992 Mar	3.6	0.9	−6	66.5	0.6	6.0	4.3	25	157.0	0.7
1311+678	1990 Mar	4.8	3.3	−84	148.0	2.0	5.8	5.0	82	184.0	2.2
1317+520	1992 Jun	1.7	1.0	−16	161.0	0.5	4.6	3.9	23	179.0	0.7
1333+459	1992 Jun	1.8	1.0	−21	350.0	0.6	4.6	3.7	4	579.0	0.6
1333+589	1992 Jun	1.6	1.0	−25	219.0	0.8	4.6	3.7	18	307.0	1.9
1342+663	1991 Jun	1.3	1.0	−28	597.0	0.4	5.0	4.5	−14	682.0	0.6
1347+539	1990 Mar	1.3	1.0	15	437.0	0.6	5.1	4.3	49	505.0	0.6
1357+769	1991 Jun	1.4	0.9	14	584.0	0.4	5.4	4.2	40	643.0	0.6
1418+546	1990 Mar	1.3	0.9	−15	1470.0	0.6	5.1	4.3	6	1930.0	1.0
1435+638	1990 Mar	1.4	0.9	79	536.0	0.6	5.9	4.0	−61	733.0	0.6
1437+624[c]	1991 Jun	1.2	1.0	−29	129.0	0.4	5.2	4.4	−4	267.0	0.6
1438+385	1992 Jun	2.2	0.9	−12	321.0	0.6	4.9	3.8	14	429.0	0.5
1504+377	1992 Jun	2.3	0.9	−13	349.0	0.5	5.0	3.8	13	534.0	0.5
1547+507	1992 Jun	1.7	1.0	−13	438.0	0.5	4.7	4.0	24	557.0	0.6
1637+626[b]	1991 Jun										
1638+398	1990 Mar	2.0	0.9	−19	1570.0	0.7	5.3	3.7	5	1760.0	1.0
1656+477	1990 Mar	1.7	0.9	−16	1230.0	0.8	5.3	3.8	14	1440.0	1.0
1656+482	1991 Sep	2.4	1.0	−18	393.0	0.3	6.5	5.2	15	566.0	0.5
1719+357	1991 Sep	3.1	1.0	−16	288.0	0.3	7.3	5.4	4	387.0	0.3
1732+389	1990 Mar	2.0	0.9	−12	1040.0	0.7	5.8	3.8	8	1230.0	1.0
1734+508	1991 Sep	1.8	1.2	−20	465.0	0.4	6.1	5.7	8	722.0	0.5
1738+476	1990 Mar	1.5	0.9	−11	797.0	0.6	5.1	4.0	14	1030.0	0.8
1751+441	1990 Mar	2.1	0.8	−18	604.0	0.6	6.7	3.8	10	843.0	0.7
1758+388	1990 Mar	2.4	0.8	−13	691.0	0.6	6.2	3.7	9	889.0	0.7
1800+440	1990 Mar	2.1	0.8	−19	389.0	0.6	6.3	3.8	5	501.0	0.7
1819+396	1990 Mar	7.8	3.1	−5	228.0	1.8	10.0	5.5	17	245.0	2.2
1842+681	1990 Mar	1.2	0.9	−50	622.0	0.8	5.0	4.2	−26	801.0	1.0
1843+356	1991 Sep	3.5	1.0	−12	245.0	0.3	7.5	5.3	14	528.0	0.4
1926+611	1990 Mar	1.4	0.9	−38	399.0	0.6	5.6	4.1	−7	551.0	0.7
1943+546	1991 Sep	1.9	1.1	−12	245.0	0.3	6.3	5.4	13	481.0	0.4
2007+777	1992 Jun	1.2	1.1	−8	1540.0	0.7	4.8	3.8	16	1950.0	0.7
2010+723	1991 Jun	1.1	1.0	−18	519.0	0.4	5.3	4.4	−4	919.0	0.5
2207+374	1991 Sep	2.9	1.0	−10	152.0	0.3	10.5	8.0	27	277.0	0.4
2214+350	1990 Mar	2.7	0.8	−14	527.0	0.5	6.7	3.7	9	586.0	0.6
2229+695	1990 Mar	1.7	0.8	−33	650.0	0.5	6.4	3.8	2	949.0	0.8
2253+417	1990 Mar	2.2	0.8	−19	624.0	0.4	6.3	3.8	9	958.0	0.7
2255+416	1990 Mar	2.0	0.9	−20	236.0	0.7	6.3	3.8	8	304.0	0.8
2311+469	1990 Mar	2.6	0.8	−17	71.8	0.5	3.1	1.2	−25	78.0	0.7

[a] The restoring beam is an elliptical Gaussian with FWHM major axis a and minor axis b, with major axis in position angle θ.
[b] Heavily resolved.
[c] The same contour levels are used for maps of individual components.

NOTES.—Col. (1): Source name. Col. (2): Observation date. Cols. (3)–(5): The beam characteristics of the naturally weighted maps. Col. (6): The peak intensity of the naturally weighted maps (mJy beam^{-1}). Col. (7): The rms noise in the naturally weighted maps (mJy beam^{-1}). Cols. (8)–(10): The beam characteristics of the tapered maps. Col. (11): The peak intensity of the tapered maps (mJy beam^{-1}). Col. (12): The rms noise in the tapered maps (mJy beam^{-1}).

Table 2 is published in computer-readable form in the AAS CD-ROM Series, Vol. 5.

TABLE 3

GAUSSIAN MODELS

Source	S (Jy)	r (mas)	θ (°)	a (mas)	b/a	ϕ (°)	Amp. A.F.	Cl.Phs. A.F.	Total A.F.
0010+405	0.423	0.00	0.0	0.55	0.40	144.8	1.004	1.059	1.029
	0.058	0.97	−30.2	1.41	0.30	−31.2			
0022+390	0.395	0.00	0.0	0.55	0.86	109.8	1.041	1.077	1.057
	0.087	5.28	168.8	9.19	0.11	153.9			
	0.118	1.04	159.6	0.68	0.41	44.8			
0102+480	0.664	0.50	194.1	1.63	0.72	11.2	1.035	1.041	1.038
	0.453	0.00	0.0	0.28	0.34	111.3			
0248+430	0.718	0.00	0.0	0.99	0.41	150.2	1.261	1.127	1.201
	0.353	1.29	145.5	0.51	0.00	61.5			
	0.044	5.43	154.3	4.80	0.00	150.5			
	0.128	11.93	140.8	1.30	0.64	10.9			
0402+379	0.403	0.65	235.0	2.90	0.78	89.6	1.017	1.354	1.172
	0.094	0.24	158.3	0.75	0.00	29.9			
	0.048	2.72	91.3	1.07	0.81	178.4			
	0.162	27.72	35.3	11.68	0.34	23.2			
0602+673	0.642	0.00	0.0	0.53	0.66	−19.7	1.052	1.061	1.056
	0.036	3.46	187.3	6.84	0.21	173.7			
0615+820	0.528	0.00	0.0	0.67	0.64	154.1	1.027	1.105	1.063
	0.254	0.84	238.9	1.12	0.56	−5.6			
0620+389	0.436	0.00	0.0	0.47	0.68	−62.2	0.949	0.997	0.971
	0.049	1.20	149.8	1.98	0.00	27.0			
	0.089	6.68	134.2	2.22	0.67	−32.9			
0642+449	1.566	0.00	0.0	0.34	0.76	82.3	0.998	0.975	0.987
	0.086	3.03	92.1	1.57	0.81	25.4			
0646+600	0.449	0.00	0.0	0.51	0.64	38.1	1.018	1.106	1.059
	0.493	3.03	−144.8	0.53	0.81	12.4			
	0.102	1.35	−139.1	1.59	0.08	12.6			
	0.012	3.39	13.0	0.58	0.33	153.8			
0650+371	1.288	0.00	0.0	0.77	0.57	43.8	1.109	1.214	1.157
	0.022	3.01	87.3	1.23	0.30	99.5			
0707+476	0.434	0.00	0.0	0.29	0.95	−52.4	1.041	1.032	1.037
	0.279	0.62	−16.0	0.44	0.68	48.7			
	0.040	5.16	23.4	2.28	0.38	134.9			
	0.087	1.80	6.1	4.19	0.21	−0.9			
	0.014	15.94	51.7	10.36	0.50	−34.7			
0716+714	0.631	0.00	0.0	0.34	0.22	28.1	1.078	1.035	1.058
	0.018	1.99	6.5	0.00	0.10	0.0			
0740+828	0.319	0.00	0.0	0.36	0.74	9.9	1.141	1.149	1.145
	0.119	0.87	10.3	0.00	0.01	105.2			
	0.258	2.76	−5.5	1.18	0.85	101.1			
	0.049	8.63	−4.2	3.10	0.29	19.4			
	0.048	17.67	−5.1	10.29	0.23	−2.7			
0746+483	0.363	0.00	0.0	0.47	0.35	93.4	1.075	1.129	1.100
	0.391	0.82	−85.4	0.74	0.59	−75.0			
	0.087	3.10	−92.4	1.52	0.60	81.3			
0755+379	0.120	0.00	0.0	0.26	0.00	54.6	1.028	1.087	1.055
	0.031	0.72	127.8	0.54	0.00	−93.8			
	0.048	1.52	119.8	2.85	0.26	118.9			
0805+410	0.956	0.00	0.0	0.42	0.60	10.4	1.127	1.002	1.071
	0.025	2.46	27.8	1.51	0.00	13.1			
	0.070	6.54	46.8	5.73	0.37	58.1			

TABLE 3—*Continued*

Source	S (Jy)	r (mas)	θ (°)	a (mas)	b/a	ϕ (°)	Amp. A.F.	Cl.Phs. A.F.	Total A.F.
0812+367	0.549	0.00	0.0	0.21	0.51	−91.3	1.089	1.043	1.069
	0.231	1.00	−12.2	0.35	0.96	−27.6			
	0.170	8.61	−9.5	9.22	0.21	−20.1			
0820+560	1.168	0.00	0.0	0.28	0.66	115.2	1.164	1.095	1.134
	0.126	0.73	97.4	0.73	0.00	59.9			
	0.133	2.63	97.6	1.93	0.47	88.7			
	0.159	18.88	75.0	12.98	0.44	90.5			
0821+394	0.597	0.00	0.0	0.29	0.95	34.0	1.305	1.068	1.205
	0.115	0.61	−22.0	0.81	0.66	−36.8			
	0.095	4.28	−44.8	1.58	0.48	133.4			
	0.257	294.64	−49.8	10.91	0.81	35.5			
0828+493	0.202	0.00	0.0	0.37	0.63	88.2	1.008	1.063	1.033
	0.070	0.74	67.6	1.27	0.71	−43.2			
	0.038	9.93	61.4	11.18	0.34	67.5			
0833+585	0.396	0.00	0.0	0.47	0.64	69.8	1.103	1.114	1.108
	0.246	0.94	85.1	0.95	0.61	61.5			
0900+428	0.175	0.00	0.0	0.20	0.86	111.1	1.039	1.064	1.051
	0.106	0.70	−62.1	0.91	0.01	−79.4			
	0.017	4.54	−79.6	0.71	0.67	−25.0			
	0.025	13.29	−76.6	1.51	0.59	−16.9			
	0.047	21.41	−67.1	2.89	0.82	142.6			
	0.098	23.20	−76.2	21.41	0.59	90.8			
0917+449	0.705	0.00	0.0	0.50	0.07	−30.5	1.020	1.031	1.025
	0.578	0.91	176.1	1.02	0.50	3.9			
	0.080	5.92	−162.7	7.07	0.44	26.1			
	0.043	19.59	−161.3	8.79	0.26	80.1			
0917+624	0.811	0.00	0.0	0.42	0.43	145.0	1.035	1.030	1.033
	0.213	0.72	−21.0	0.60	0.18	20.6			
	0.236	5.56	−18.6	2.57	0.78	−19.5			
	0.042	20.78	−25.9	10.72	0.64	27.1			
0955+476	1.051	0.00	0.0	0.33	0.80	114.6	0.988	1.008	0.997
	0.022	1.85	132.6	2.08	0.56	144.3			
1003+830	0.278	0.00	0.0	0.51	0.26	71.1	1.056	1.040	1.049
	0.041	2.67	83.1	1.10	0.00	64.5			
	0.111	5.88	85.1	2.20	0.43	114.3			
	0.048	18.98	96.5	14.04	0.63	104.0			
1015+359	0.426	0.00	0.0	0.13	0.00	87.3	1.143	1.028	1.092
	0.176	0.82	187.0	0.55	0.66	39.0			
	0.099	2.75	181.9	1.51	0.46	175.7			
1020+400	0.694	0.00	0.0	0.21	0.01	−69.7	1.150	1.055	1.108
	0.118	2.73	−40.7	3.13	0.23	−41.9			
	0.060	12.14	−33.9	7.11	0.41	−22.8			
1030+415	0.223	0.00	0.0	0.00	1.00	120.6	1.040	1.033	1.036
	0.060	0.69	−4.5	0.41	0.15	−56.9			
	0.073	3.70	3.8	4.50	0.33	9.7			
	0.035	8.95	−15.0	14.76	0.09	−17.4			
1039+811	0.833	0.00	0.0	0.30	0.40	−60.3	1.183	1.010	1.107
	0.244	0.83	−64.8	0.81	0.40	−63.8			
	0.072	2.56	−68.2	1.19	0.55	−89.2			
	0.043	6.10	−78.0	5.70	0.28	−88.1			
1044+719	0.234	0.00	0.0	0.00	1.00	−54.4	1.041	1.019	1.031
	0.737	0.36	113.2	0.69	0.93	−36.3			

TABLE 3—*Continued*

Source	S (Jy)	r (mas)	θ (°)	a (mas)	b/a	ϕ (°)	Amp. A.F.	Cl.Phs. A.F.	Total A.F.
1053+704	0.269	0.00	0.0	0.29	0.94	172.2	1.047	1.017	1.033
	0.264	0.25	199.5	0.44	0.57	13.8			
	0.043	1.62	−144.5	1.83	0.40	56.3			
1053+815	0.372	0.00	0.0	0.19	0.98	178.1	1.033	1.030	1.032
	0.175	0.21	−143.0	0.76	0.35	−140.8			
	0.017	1.61	−129.8	1.66	0.62	150.4			
1058+726	0.122	0.00	0.0	0.59	0.26	−3.1	1.015	1.172	1.090
	0.034	0.76	−4.7	0.00	1.00	0.0			
	0.101	1.95	3.2	0.59	0.00	−127.3			
	0.148	3.40	9.9	0.95	0.62	23.7			
	0.024	23.74	19.8	4.81	0.44	−1.2			
1101+384	0.366	0.00	0.0	0.32	0.54	142.1	1.126	1.069	1.101
	0.072	1.39	−24.1	3.40	0.26	−21.8			
	0.144	42.16	−52.6	80.97	0.41	−68.9			
1128+385	0.759	0.00	0.0	0.70	0.04	3.4	1.032	1.011	1.023
	0.191	0.73	−136.1	1.03	0.41	−1.9			
	0.055	3.34	−81.0	7.72	0.58	−49.1			
1138+594	0.087	0.00	0.0	0.00	0.07	−97.4	0.928	1.224	1.068
	0.019	15.57	162.0	1.96	0.28	13.0			
	0.147	225.41	171.7	24.02	0.39	61.2			
1144+402	0.457	0.00	0.0	0.06	0.96	153.1	1.036	1.027	1.032
	0.087	2.70	−0.0	4.00	0.56	2.4			
	0.095	0.65	1.0	0.63	0.87	58.5			
1144+542	0.162	0.00	0.0	0.00	1.00	12.2	0.996	1.079	1.035
	0.044	0.60	177.1	0.12	0.00	−3.5			
	0.121	1.10	177.7	0.85	0.70	−2.3			
	0.060	2.63	196.3	1.92	0.37	122.9			
1150+497	0.327	0.00	0.0	0.46	0.22	25.1	1.044	1.068	1.055
	0.149	1.55	−157.5	0.75	0.22	23.4			
	0.037	9.41	−156.0	14.62	0.17	−154.3			
1150+812	0.702	0.00	0.0	0.36	0.43	−4.3	0.987	1.009	0.997
	0.316	0.99	182.1	0.53	0.54	136.7			
	0.188	2.97	168.4	2.74	0.38	150.2			
	0.036	7.60	144.5	8.28	0.26	133.6			
1213+350	0.420	0.00	0.0	0.72	0.00	−70.9	1.064	1.104	1.082
	0.325	1.15	204.3	2.44	0.59	138.4			
	0.233	3.38	117.3	9.51	0.44	46.6			
	0.025	36.84	−125.5	0.97	0.00	36.3			
1216+487	0.265	0.00	0.0	0.13	0.00	30.5	1.000	1.065	1.030
	0.287	1.48	102.1	2.00	0.25	100.1			
	0.066	4.95	103.9	8.12	0.24	116.2			
1225+368	0.351	0.00	0.0	1.37	0.73	−153.4	1.154	1.341	1.241
	0.240	2.27	−32.8	1.78	0.45	−16.1			
	0.117	18.48	−78.1	2.41	0.30	−101.8			
	0.050	25.08	−80.0	1.62	0.00	−71.9			
	0.062	31.80	−80.7	2.10	0.00	89.0			
	0.040	54.78	−85.5	4.75	0.69	−29.3			
1242+410	0.116	0.00	0.0	0.78	0.92	152.3	1.005	1.526	1.261
	0.152	7.81	25.7	4.86	0.20	24.6			
	0.160	21.11	29.4	4.79	0.74	37.2			
	0.056	3.37	−140.8	1.64	0.24	131.2			
	0.229	8.66	−154.8	9.33	0.76	−23.8			

TABLE 3—*Continued*

Source	S (Jy)	r (mas)	θ (°)	a (mas)	b/a	ϕ (°)	Amp. A.F.	Cl.Phs. A.F.	Total A.F.
1311+678	0.166	0.00	0.0	1.43	0.41	67.4	1.141	1.892	1.504
	0.157	4.66	−67.2	5.07	0.45	−83.8			
	0.410	37.12	−121.0	11.13	0.74	−13.2			
	0.065	41.35	144.6	3.50	0.00	165.5			
	0.035	29.12	175.0	5.26	0.28	34.7			
1317+520	0.181	0.00	0.0	0.47	0.38	116.5	0.985	1.078	1.029
	0.067	4.52	124.4	2.91	0.35	135.5			
	0.007	19.90	129.9	3.46	0.00	6.6			
1333+459	0.345	0.00	0.0	0.82	0.33	113.2	1.058	1.178	1.115
	0.298	1.19	−62.7	1.16	0.26	108.4			
1333+589	0.097	0.00	0.0	0.50	0.71	−44.9	1.140	1.304	1.218
	0.227	0.01	−108.9	1.21	0.64	−35.1			
	0.325	12.73	−161.7	1.69	0.67	117.4			
1342+663	0.685	0.00	0.0	0.48	0.80	110.8	1.058	1.005	1.034
	0.007	2.78	107.6	1.66	0.00	−35.7			
	0.006	4.79	81.1	1.47	0.01	−21.1			
1347+539	0.419	0.00	0.0	0.23	0.00	−53.4	1.111	1.048	1.083
	0.034	0.84	145.0	0.01	0.49	4.7			
	0.063	1.44	141.2	1.76	0.00	132.2			
	0.072	5.41	141.0	3.86	0.20	−41.9			
	0.102	15.98	128.2	13.82	0.34	105.0			
	0.094	58.94	141.3	16.12	0.75	37.4			
1357+769	0.635	0.00	0.0	0.34	0.86	125.3	1.027	1.025	1.026
	0.025	2.87	−111.2	2.84	0.10	−5.5			
1418+546	1.470	0.00	0.0	0.34	0.42	−68.8	1.097	1.042	1.073
	0.415	1.07	129.3	0.55	0.56	110.6			
	0.230	2.92	128.2	4.34	0.35	128.5			
	0.083	16.59	121.0	9.25	0.86	72.3			
1435+638	0.418	0.00	0.0	0.75	0.38	63.6	1.166	1.125	1.148
	0.241	0.46	−134.8	0.00	0.00	133.5			
	0.202	2.61	−125.9	1.64	0.25	26.6			
	0.124	9.08	−144.6	0.94	0.70	52.1			
	0.006	22.41	−133.4	1.97	0.05	30.0			
1437+624	0.193	0.00	0.0	1.01	0.65	105.5	1.068	1.286	1.172
	0.093	2.11	−74.5	2.58	0.62	100.4			
	0.183	5.74	−68.3	13.29	0.23	−35.8			
	0.058	104.24	170.4	2.47	0.15	65.1			
	0.198	103.32	169.9	4.53	0.49	63.2			
	0.057	6.64	−93.9	2.72	0.62	−5.4			
1438+385	0.244	0.00	0.0	0.33	0.78	47.2	1.025	1.073	1.048
	0.140	0.72	8.9	1.03	0.69	−5.6			
	0.093	2.24	−13.8	2.01	0.50	−0.4			
	0.106	8.15	−12.0	6.74	0.26	−2.5			
1504+377	0.413	7.07	44.9	0.67	0.15	37.0	0.989	1.066	1.025
	0.116	5.92	45.4	0.00	0.30	42.0			
	0.149	0.57	40.3	11.28	0.16	45.2			
1547+507	0.430	0.00	0.0	0.18	0.85	168.6	1.052	1.044	1.048
	0.088	1.01	−152.1	0.79	0.00	3.8			
	0.159	3.50	−147.2	1.78	0.28	41.0			
	0.106	7.26	−130.5	1.13	0.41	−0.2			
	0.063	5.84	−136.4	1.58	0.21	71.1			
1638+398	1.752	0.00	0.0	0.47	0.85	−41.0	1.103	1.056	1.083
	0.034	1.40	−58.4	2.54	0.00	11.2			

TABLE 3—*Continued*

Source	S (Jy)	r (mas)	θ (°)	a (mas)	b/a	ϕ (°)	Amp. A.F.	Cl.Phs. A.F.	Total A.F.
1656+477	1.122	0.00	0.0	0.56	0.49	−1.5	1.138	1.085	1.115
	0.325	0.51	1.9	0.86	0.60	−24.4			
	0.063	4.38	−25.5	3.38	0.28	−46.1			
	0.043	5.86	−18.7	0.99	0.83	28.7			
1656+482	0.392	0.00	0.0	0.37	0.00	84.8	1.084	1.052	1.069
	0.116	0.81	−108.6	0.29	0.00	−16.7			
	0.046	0.94	−108.4	1.40	0.00	−119.9			
	0.036	3.27	−104.5	6.41	0.41	−111.0			
	0.059	7.50	−98.8	9.87	0.56	82.1			
1719+357	0.212	0.00	0.0	0.00	1.00	0.0	1.045	1.028	1.037
	0.103	0.93	184.0	0.00	0.50	0.0			
	0.138	4.27	178.3	2.06	0.28	−1.5			
1732+389	0.995	0.00	0.0	0.52	0.52	174.1	1.278	1.062	1.187
	0.234	0.54	105.6	0.00	0.50	100.0			
1734+508	0.416	0.00	0.0	0.41	0.87	−121.7	1.182	1.162	1.173
	0.188	0.88	21.7	0.61	0.72	−174.1			
	0.223	3.36	19.3	1.02	0.67	30.4			
1738+476	0.924	0.00	0.0	0.59	0.47	51.2	0.915	1.113	1.008
	0.139	1.05	−86.4	0.64	0.83	9.0			
	0.017	2.70	−94.2	0.73	0.46	50.8			
1751+441	0.695	0.00	0.0	0.53	0.67	80.3	1.088	1.041	1.067
	0.232	1.48	87.3	1.39	0.53	−82.2			
	0.026	8.30	80.5	8.44	0.63	79.8			
1758+388	0.828	0.00	0.0	0.60	0.53	82.3	1.051	1.082	1.065
	0.091	1.05	−99.1	1.23	0.00	79.1			
1800+440	0.331	0.00	0.0	0.17	0.68	73.4	1.045	1.058	1.051
	0.090	0.52	−160.0	0.33	0.00	44.7			
	0.088	1.36	−156.8	0.65	0.62	−177.0			
	0.047	14.58	−155.7	30.54	0.10	24.3			
1819+396	0.273	0.00	0.0	1.61	0.43	−56.5	1.435	1.414	1.426
1842+681	0.647	0.00	0.0	0.45	0.57	107.0	1.149	1.075	1.117
	0.181	1.32	134.3	1.31	0.53	−28.0			
	0.024	3.64	148.4	6.96	0.09	−35.5			
1843+356	0.173	0.00	0.0	0.49	0.98	51.9	1.075	1.251	1.159
	0.116	0.91	53.5	0.62	0.45	3.1			
	0.313	7.06	43.3	1.29	0.70	157.8			
	0.101	5.15	43.8	1.58	0.50	39.6			
	0.140	8.30	45.6	1.67	0.03	54.2			
1926+611	0.394	0.00	0.0	0.43	0.72	121.2	1.038	1.091	1.062
	0.133	0.94	118.7	0.73	0.22	130.4			
	0.049	1.53	141.0	1.88	0.53	166.0			
	0.024	6.76	179.6	2.64	0.69	102.5			
	0.008	12.83	−145.8	0.69	0.02	3.5			
1943+546	0.024	0.00	0.0	6.18	0.06	125.7	1.161	1.170	1.165
	0.234	16.80	−91.8	0.63	0.69	63.1			
	0.248	15.33	−91.0	2.98	0.27	−98.0			
	0.184	13.07	−79.8	7.42	0.85	2.0			
	0.038	19.06	85.9	4.70	0.74	75.1			
	0.122	23.11	85.0	2.00	0.78	161.3			
	0.118	24.13	84.7	0.49	0.00	74.1			
2007+777	1.698	0.00	0.0	0.45	0.49	73.8	1.098	1.040	1.071
	0.268	1.00	−107.5	0.00	0.00	−117.2			
	0.124	3.90	−94.5	5.23	0.25	−99.9			
	0.023	17.68	−97.0	3.18	0.50	−171.8			

TABLE 3—*Continued*

Source	S (Jy)	r (mas)	θ (°)	a (mas)	b/a	ϕ (°)	Amp. A.F.	Cl.Phs. A.F.	Total A.F.
2010+723	0.350	0.00	0.0	0.27	0.00	−36.4	1.071	1.088	1.079
	0.142	0.23	−25.1	1.29	0.00	−30.4			
	0.426	0.99	−39.2	0.82	0.47	110.5			
	0.021	2.52	−128.1	1.61	0.00	111.5			
	0.089	3.93	−118.6	7.44	0.47	27.7			
2207+374	0.143	0.00	0.0	0.57	0.34	45.4	1.080	1.169	1.121
	0.048	0.57	−140.6	1.28	0.00	−129.1			
	0.073	5.24	−133.6	1.43	0.52	8.1			
	0.090	14.98	−138.9	2.47	0.57	−40.8			
	0.238	14.92	−134.3	8.36	0.47	−153.5			
	0.048	21.89	−130.2	12.74	0.26	−84.8			
	0.187	57.08	−105.7	48.57	0.55	116.0			
2214+350	0.551	0.00	0.0	0.35	0.82	−22.1	1.015	1.038	1.026
	0.049	1.96	169.4	1.13	0.55	−30.3			
2229+695	0.523	0.00	0.0	0.44	0.97	28.2	1.027	1.053	1.039
	0.456	0.56	−108.3	0.87	0.26	81.5			
	0.003	2.66	79.1	0.01	0.49	20.0			
2253+417	0.507	0.00	0.0	0.81	0.18	28.0	1.075	1.059	1.068
	0.487	1.33	−10.6	1.24	0.42	−25.7			
	0.042	4.63	21.1	1.16	0.33	47.8			
	0.064	6.65	36.3	4.11	0.35	12.3			
2255+416	0.242	0.00	0.0	0.65	0.34	−17.2	1.125	1.152	1.137
	0.054	1.13	170.3	2.15	0.36	−27.2			
	0.050	5.09	167.4	1.70	0.23	−61.2			
	0.180	8.85	165.1	3.23	0.52	−36.9			
	0.276	19.13	172.8	8.70	0.59	16.1			
	0.138	31.96	−151.5	14.69	0.65	70.3			
	0.193	42.24	−136.6	8.28	0.55	152.5			
2311+469	0.055	0.00	0.0	0.39	0.00	114.4	0.979	1.350	1.152
	0.039	0.31	121.9	0.42	0.68	6.1			
	0.012	1.72	133.9	1.66	0.65	173.2			

NOTE.—Parameters of each Gaussian component of the model brightness distribution; S, flux density; r, θ, polar coordinates of the center of the component relative to an arbitrary origin, with polar angle measured from north through east; a, b, major and minor axes of the FWHM contour; ϕ, position angle of the major axis measured from north through east. The sources 0218+357 and 0404+768 are too complicated to model.

Table 3 is published in computer-readable form in the AAS CD-ROM Series, Vol. 5.

TABLE 4

MERLIN MAP PARAMETERS

Source	Sample	Beam[a]			S_{peak}	rms
		a (mas)	b (mas)	θ (°)		
0707+476	CJ1	49.7	37.8	37	948	1.52
0812+367	CJ1	100.0	100.0	0	747	0.23
0814+425	PR	56.8	37.7	30	906	0.59
0820+560	CJ1	51.2	37.8	26	1753	0.52
0900+428	CJ1	49.0	41.0	44	376	0.23
		100.0	100.0	0	430	0.15
0917+624	CJ1	48.5	38.2	30	1059	0.46
0945+408	PR	53.4	38.8	33	1232	0.82
		100.0	100.0	0	1317	0.47
0954+556	PR	47.7	38.1	32	967	0.91
1039+811	CJ1	47.0	40.9	7	1000	0.36
1150+812	CJ1	47.3	38.5	26	979	0.32
1347+539	CJ1	44.2	36.3	−48	592	0.33
1418+546	CJ1	44.0	36.0	−48	1429	0.49
1633+382	PR	47.5	38.9	33	2113	0.94
1638+398	CJ1	48.4	38.7	31	1230	0.68
1749+701	PR	47.6	37.7	8	469	0.44
1800+440	CJ1	63.7	43.7	−37	402	0.20
		100.0	100.0	0	412	0.21
1803+784	PR	47.0	38.6	−64	1951	0.56
1819+396	CJ1	56.9	41.1	−39	324	0.53
1943+546	CJ1	50.6	38.9	24	655	0.58
1954+513	PR	50.0	38.1	25	1403	0.51

[a] The restoring beam is an elliptical Gaussian with FWHM major axis a and minor axis b, with major axis in position angle θ.

NOTES.—Col. (1): Source name. Col. (2): Sample. Cols. (3)–(5): The beam characteristics of the maps. Cols. (6)–(7): The peak intensity and rms noise of the maps (mJy beam^{-1}).

Table 4 is published in computer-readable form in the AAS CD-ROM Series, Vol. 5.

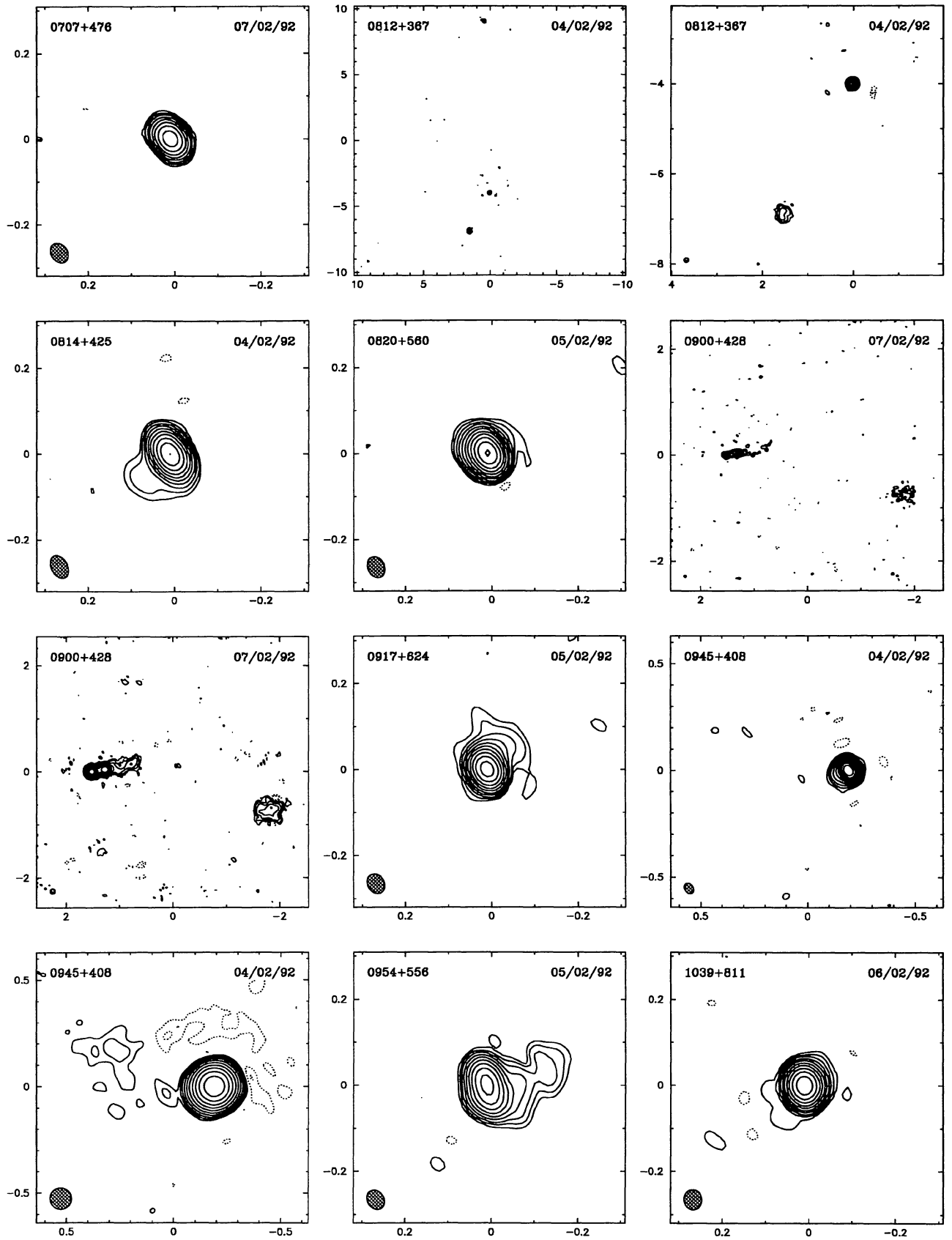

FIG. 4.—The 5 GHz MERLIN uniformly weighted maps of 20 objects. Logarithmic contour levels are used in all maps, at $-2, -1, 1, 2, 4, 8, 16, \cdots 1024 \times 3\ \sigma$ (where σ is the rms noise measured in a blank region of the map). The FWHM contour of the elliptical Gaussian restoring beam is shown hatched in the lower left-hand corner. For 0812+367, 0900+428, 0945+408, and 1800+440, which have large angular sizes, the naturally weighted map restored with a circular beam of FWHM 100 mas is also shown. In addition, an enlarged map of 0812+367 is presented to show the central and southern components in more detail. The peak intensity, rms noise, and parameters of the restoring beam are listed in Table 5. The angular scale is marked in arcseconds. FITS images corresponding to the maps presented in Fig. 4 are published in the AAS CD-ROM Series, Vol. 5.

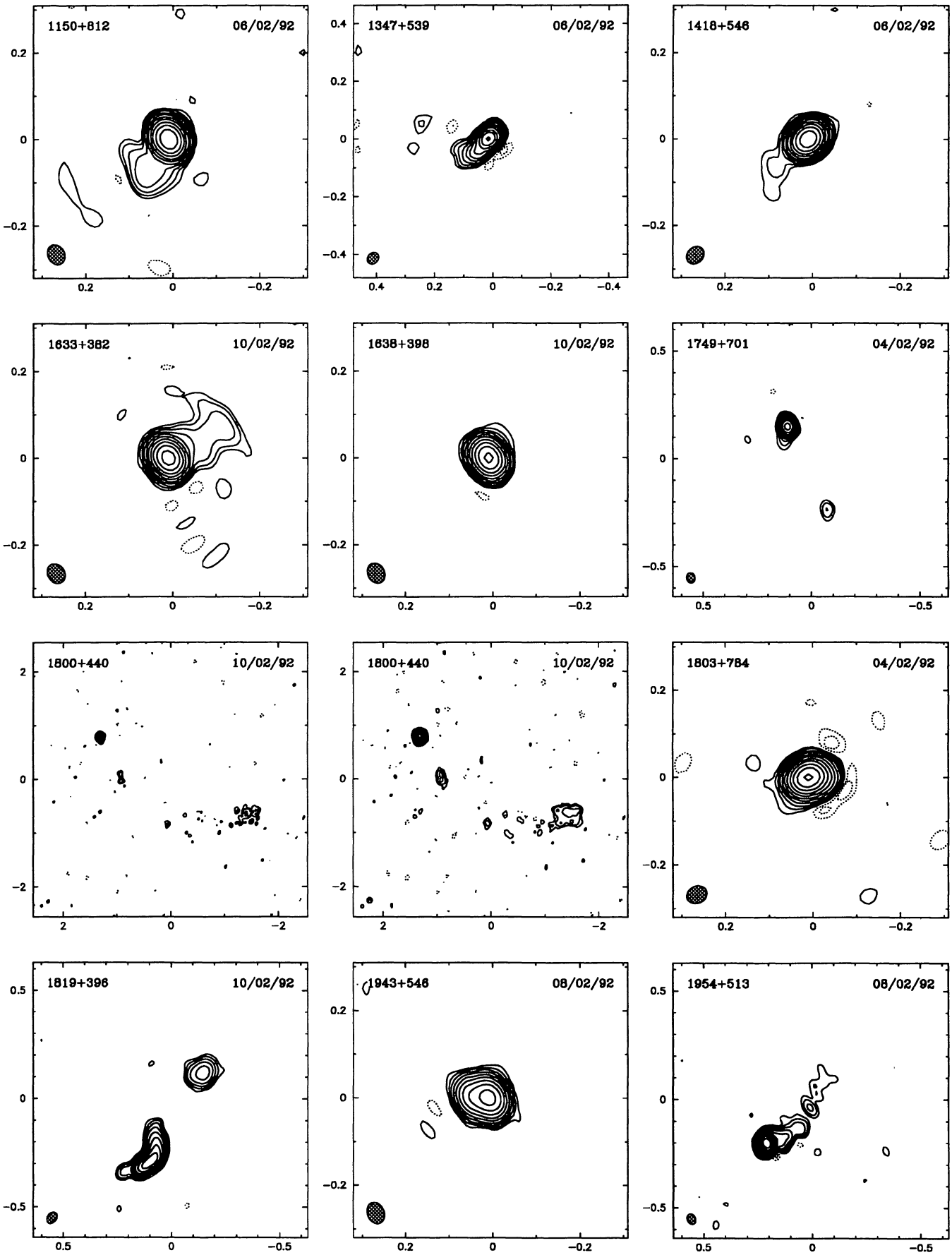

FIG. 4—*Continued*

TABLE 5

VLA MAP PARAMETERS

Source	Sample	S_{peak} (mJy)	rms (mJy)	Structure
0010+775	CJ1	1979.8	0.36	E
0016+731	PR	969.0	0.21	E?[a]
0022+390	CJ1	738.9	0.18	E
0102+480	CJ1	751.9	0.17	U
0133+476	PR	1172.8	0.41	U
0153+744	PR	1794.3	0.29	U
0212+735	PR	2443.6	0.36	U
0248+430	CJ1	1052.3	0.18	E
0309+390	CJ1	68.5	0.35	E[c]
0402+379	CJ1	1092.3	0.21	E
0404+768	PR	5639.2	0.82	U
0454+844	PR	392.1	0.10	U
0602+673	CJ1	519.1	0.18	U
0620+389	CJ1	834.3	0.27	E?
0642+449	CJ1	475.6	0.15	U
0650+371	CJ1	836.6	0.20	U
0703+426	CJ1	39.8	0.50	E[d]
0707+689	CJ1	1450.5	0.42	E
0710+439	PR	2005.3	0.28	U
0740+828	CJ1	1325.7	0.54	E
0746+483	CJ1	704.1	0.22	U
0755+379	CJ1	149.6	0.60	E[f]
0755+379	CJ1	208.3	0.64	E[e]
0805+410	CJ1	528.4	0.22	E
0818+472	CJ1	101.1	0.53	E
0821+394	CJ1	1257.0	0.56	E
0827+378	CJ1	1755.1	0.29	E
0827+378	CJ1	1920.2	0.37	E[c]
0831+557	PR	8064.7	1.28	E
0844+540	CJ1	22.9	0.36	E[c]
0900+428	CJ1	811.1	0.43	E
0917+449	CJ1	913.7	0.18	E
0945+664	CJ1	1490.7	0.24	E
0954+658	PR	636.6	0.29	E
0955+476	CJ1	650.3	0.37	U
1003+351	PR	2824.6	0.70	E[g]
1003+830	CJ1	476.3	0.15	E
1015+359	CJ1	622.0	0.31	E
1020+400	CJ1	680.6	0.21	E
1030+415	CJ1	417.8	0.16	E
1031+567	PR	1815.6	0.32	U
1044+719	CJ1	785.9	0.19	E
1053+704	CJ1	441.4	0.11	E
1053+815	CJ1	392.9	0.13	E
1058+726	CJ1	748.4	0.21	E
1101+384	CJ1	626.2	0.17	E
1138+594	CJ1	1982.0	0.43	E
1144+542	CJ1	373.4	0.14	U
1216+487	CJ1	616.9	0.15	E
1225+368	CJ1	2072.2	0.43	U
1242+410	CJ1	1366.1	0.28	U
1254+476	PR	2414.1	0.64	E
1311+678	CJ1	2427.1	0.35	E?
1333+459	CJ1	253.9	0.18	U
1333+589	CJ1	305.3	0.26	U
1336+391	CJ1	97.7	0.37	E
1342+663	CJ1	581.5	0.26	E?
1347+539	CJ1	935.2	0.21	E
1357+769	CJ1	471.0	0.12	U
1358+624	PR	4426.1	0.54	U
1437+624	CJ1	2322.4	0.32	E?
1438+385	CJ1	580.0	0.17	E
1547+507	CJ1	624.3	0.11	E?
1557+708	CJ1	24.1	0.20	E
1609+660	PR	2813.5	0.93	E
1624+416	PR	1632.4	0.89	E
1634+628	PR	4900.0	0.63	E?[h]
1638+398	CJ1	1118.2	0.31	E
1652+398	PR	1428.2	0.25	E
1656+482	CJ1	788.1	0.16	E
1719+357	CJ1	402.6	0.25	E
1732+389	CJ1	992.4	0.15	U
1734+508	CJ1	485.1	0.28	U
1738+476	CJ1	848.1	0.15	E?[b]
1749+701	PR	725.8	0.15	E
1751+441	CJ1	554.0	0.17	E
1758+388	CJ1	281.7	0.74	E
1800+440	CJ1	450.6	0.39	E
1833+653	CJ1	200.5	0.50	E
1842+681	CJ1	886.0	0.13	E
1843+356	CJ1	947.3	0.22	U
1926+611	CJ1	825.4	0.15	E?
1943+546	CJ1	1710.3	0.24	U
1954+513	PR	1377.3	0.47	E
2010+723	CJ1	1388.3	0.26	E
2021+614	PR	2169.8	0.32	U
2207+374	CJ1	1674.2	0.28	E
2214+350	CJ1	363.6	0.19	E
2229+695	CJ1	757.1	0.12	E
2253+417	CJ1	1333.7	0.29	U
2255+416	CJ1	2069.3	0.34	U
2342+821	PR	3736.2	0.47	E?[h]
2351+456	PR	1684.5	0.28	E?[h]
2352+495	PR	2515.8	0.34	U

[a] Faint component ~12″ to the north.
[b] Faint component ~1′ to the west.
[c] Logarithmic contour levels in steps of $\sqrt{2}$.
[d] Convolved with 3″ circular Gaussian beam.
[e] Convolved with 5″ circular Gaussian beam.
[f] The lowest contour is 2 σ.
[g] The lowest contour is 4 σ.
[h] Source resolved at long baselines.

NOTES.—Col. (1): Source name. Col. (2): Sample. Cols. (3)–(4): The peak intensity and rms noise in the map, in mJy beam^{-1}. Col. (5): Structure: U, unresolved; E, extended structure detected; E?, hint of extended structure (see notes).

Table 5 is published in computer-readable form in the AAS CD-ROM Series, Vol. 5.

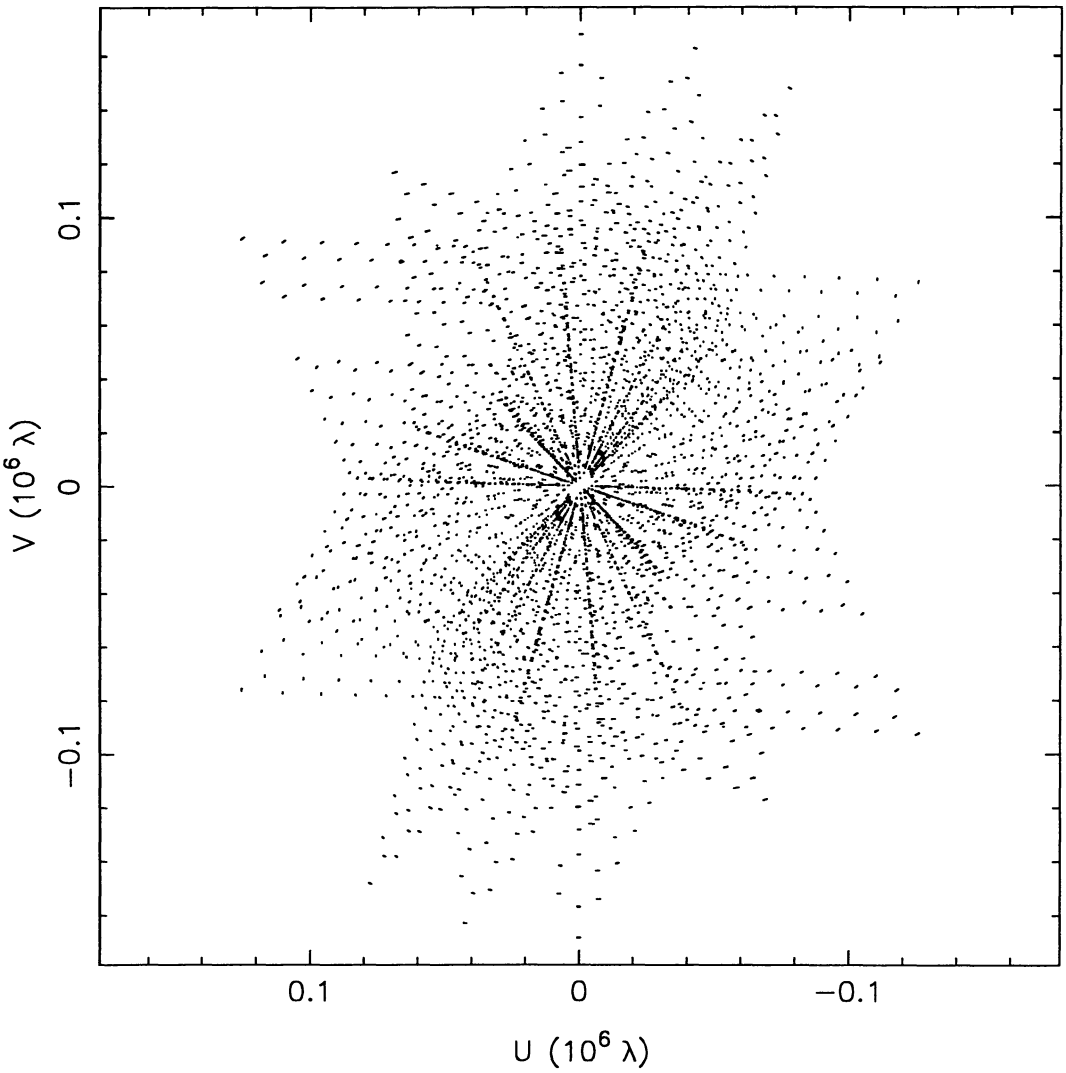

FIG. 5.—Typical *uv* coverage for VLA observations: $\delta \simeq 41°$ (1242+410 observed on 1992 November 5 at 1.365 GHz).

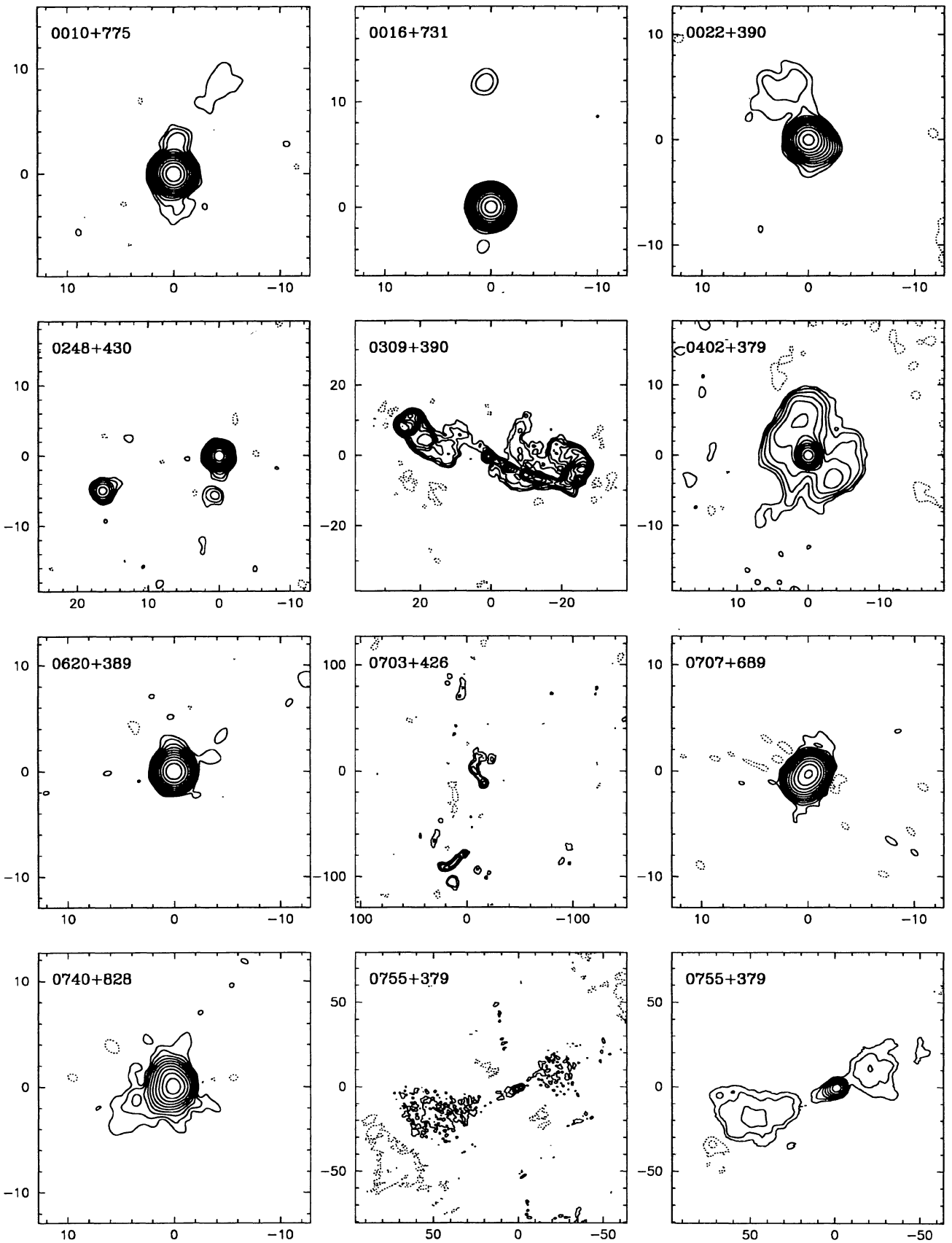

FIG. 6.—The 1.4 GHz VLA maps of 64 objects with extended structure. The naturally weighted map is shown for each object. Unless noted otherwise in Table 6, logarithmic contour levels are used in all maps, drawn at $-2, -1, 1, 2, 4, 8, 16, \cdots 1024 \times 3\ \sigma$ (where σ is the rms noise measured in a blank region of the map), and the maps are restored with a circular Gaussian beam of FWHM 1".5. For 0755+379 and 0827+378, the map restored with a larger beam is also shown. The peak intensity and rms noise are given in Table 6. The angular scale is marked in arcseconds. FITS images corresponding to the maps presented in Fig. 6 are published in the AAS CD-ROM Series, Vol. 5.

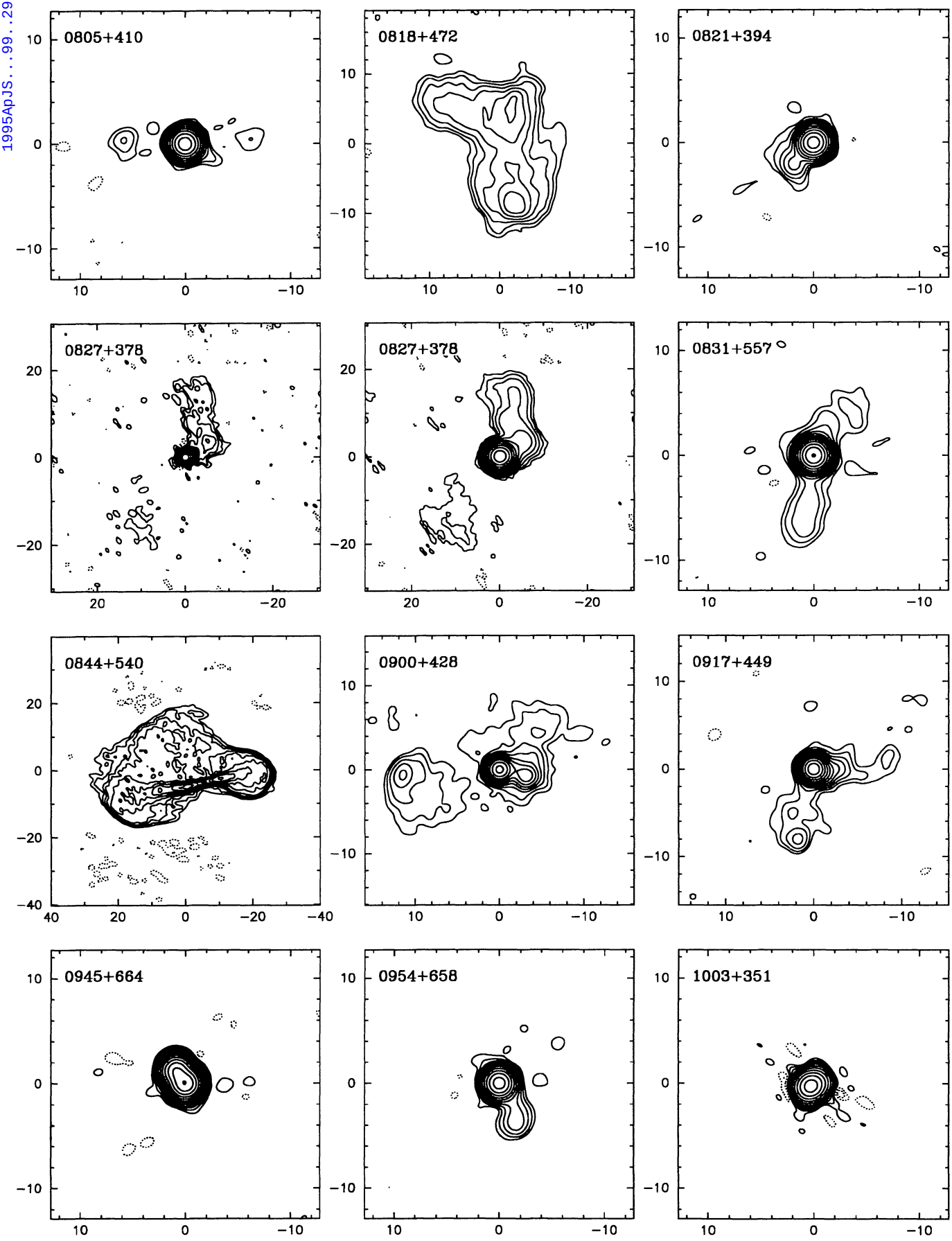

FIG. 6—*Continued*

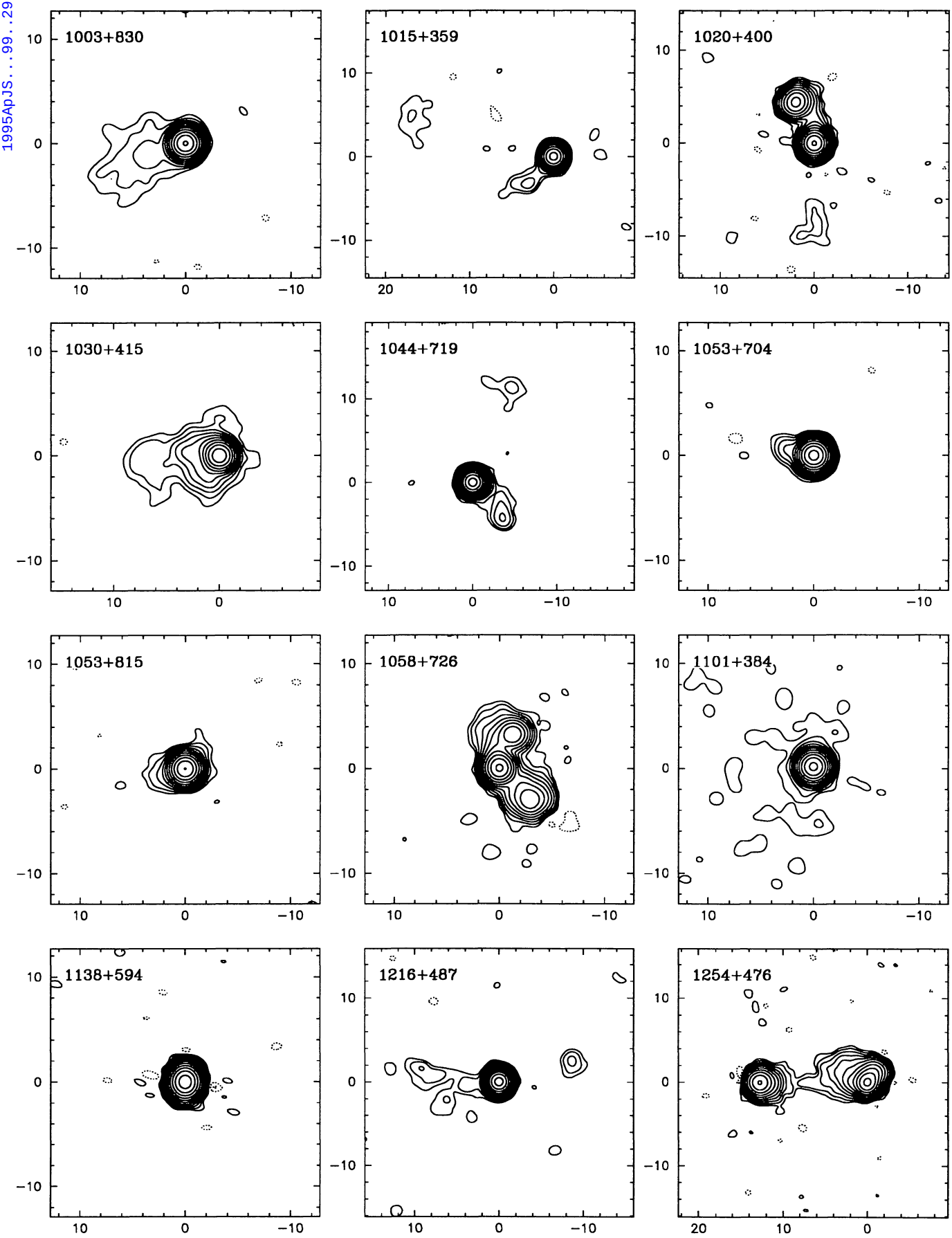

FIG. 6—*Continued*

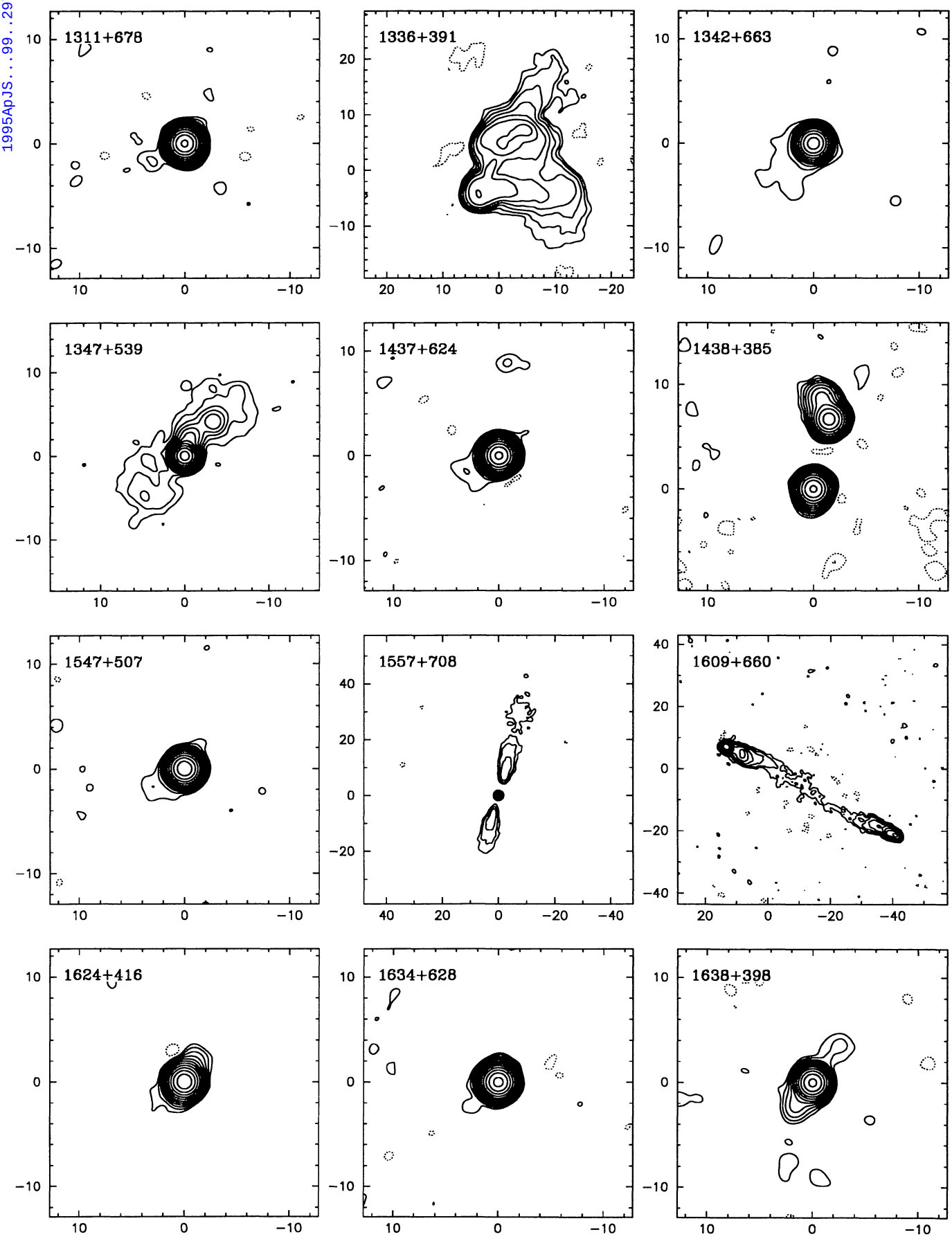

FIG. 6—*Continued*

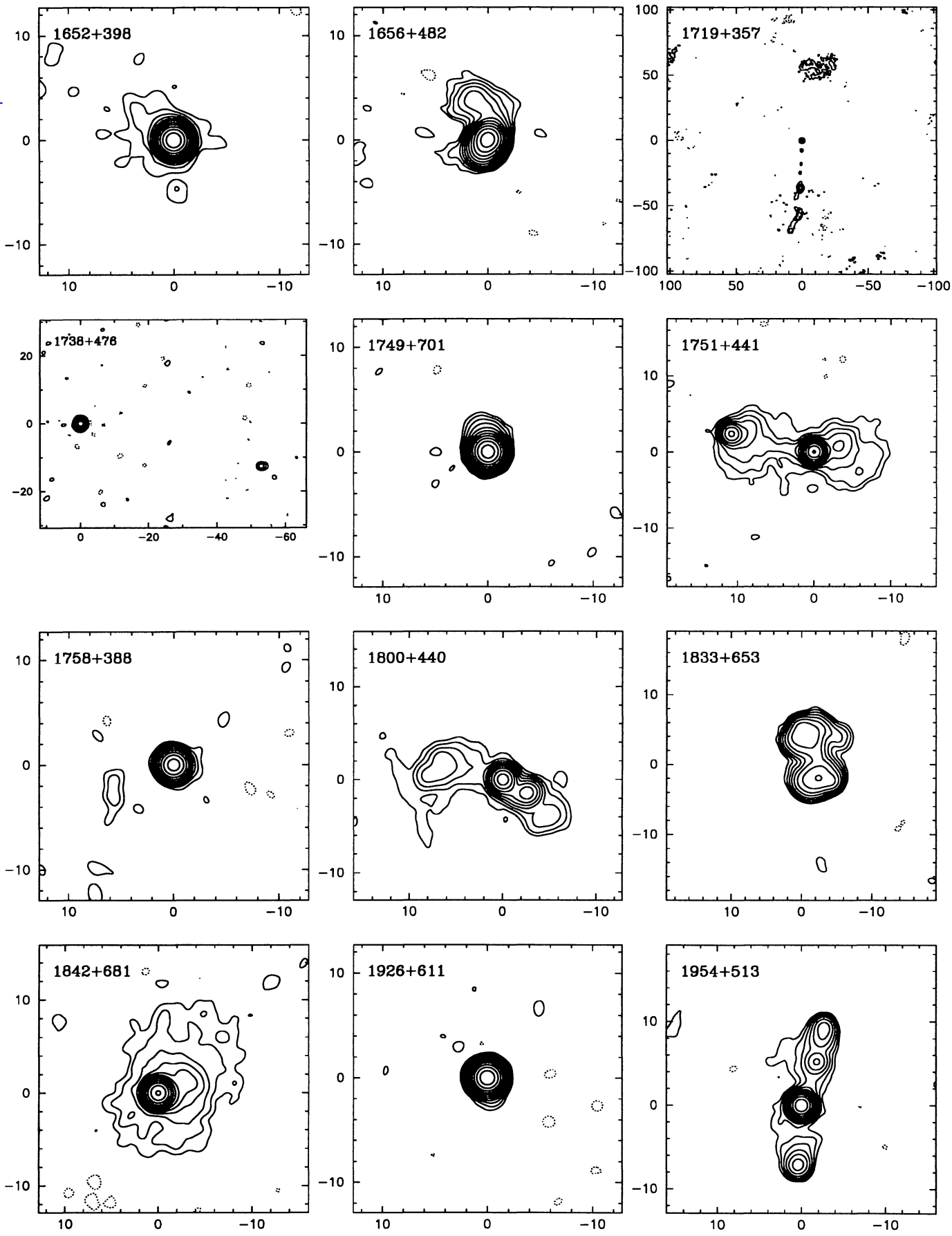

FIG. 6—*Continued*

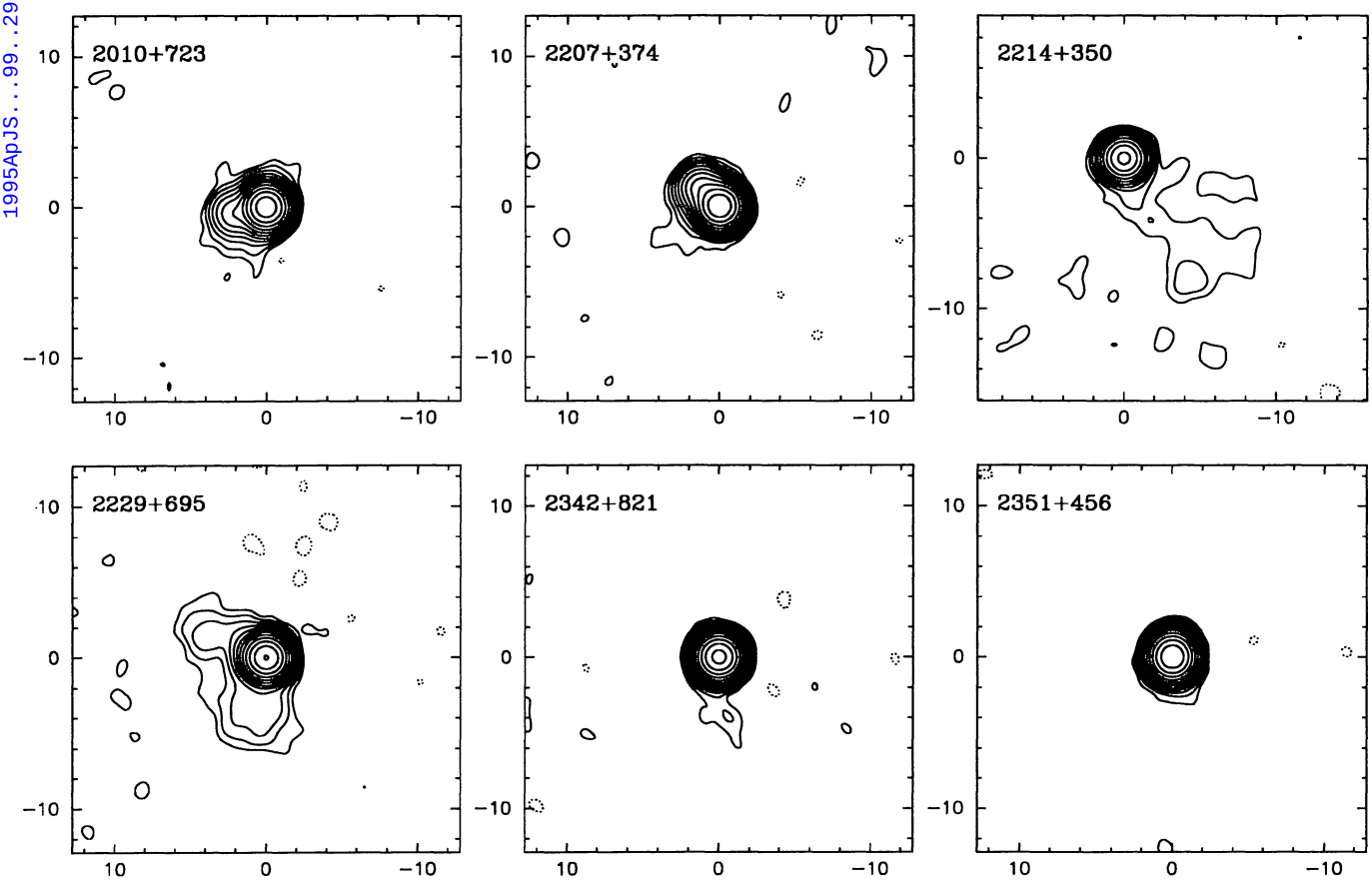

FIG. 6—*Continued*

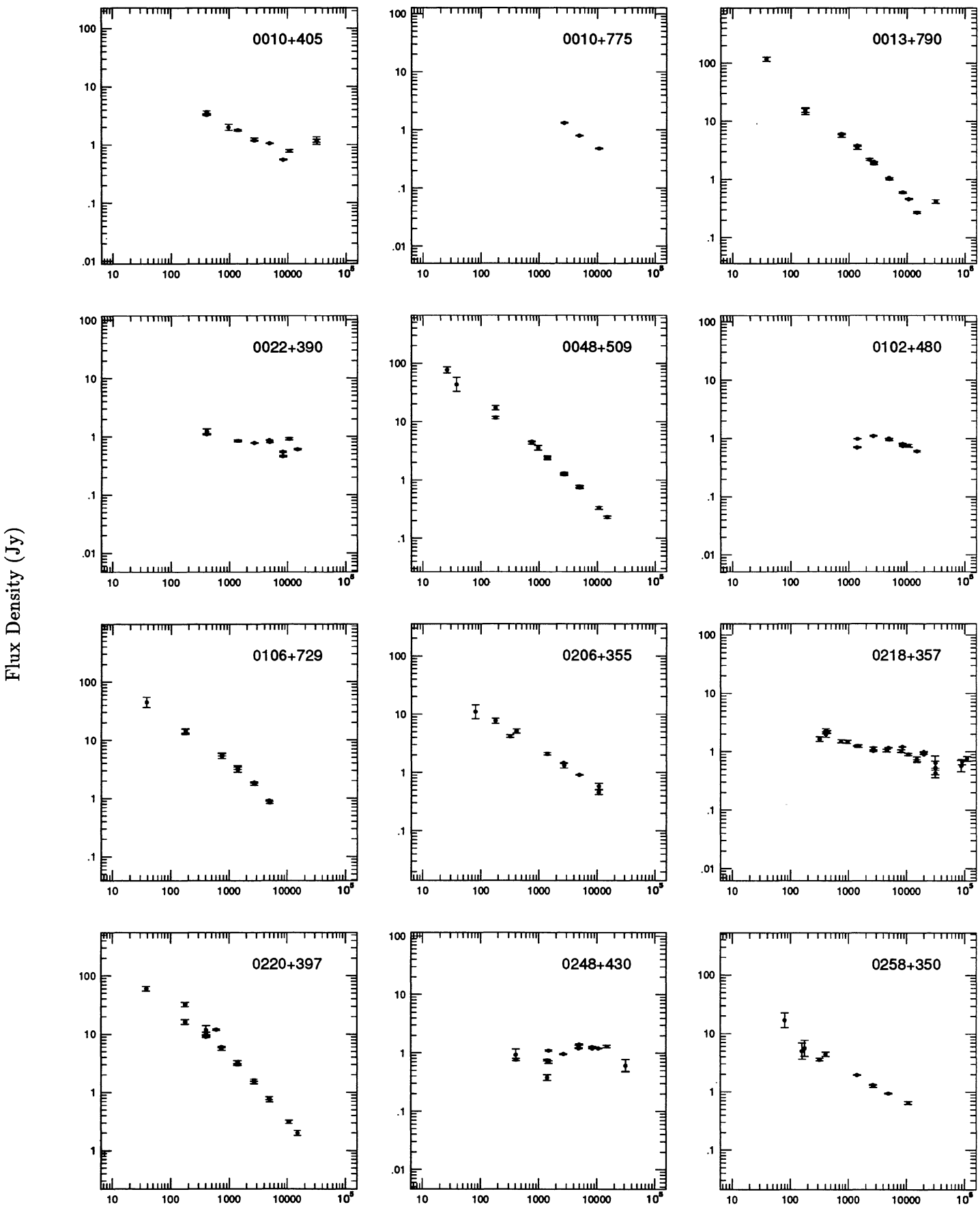

FIG. 7.—Spectra of all objects in the CJ1 sample. The data points are from the references cited in the text.

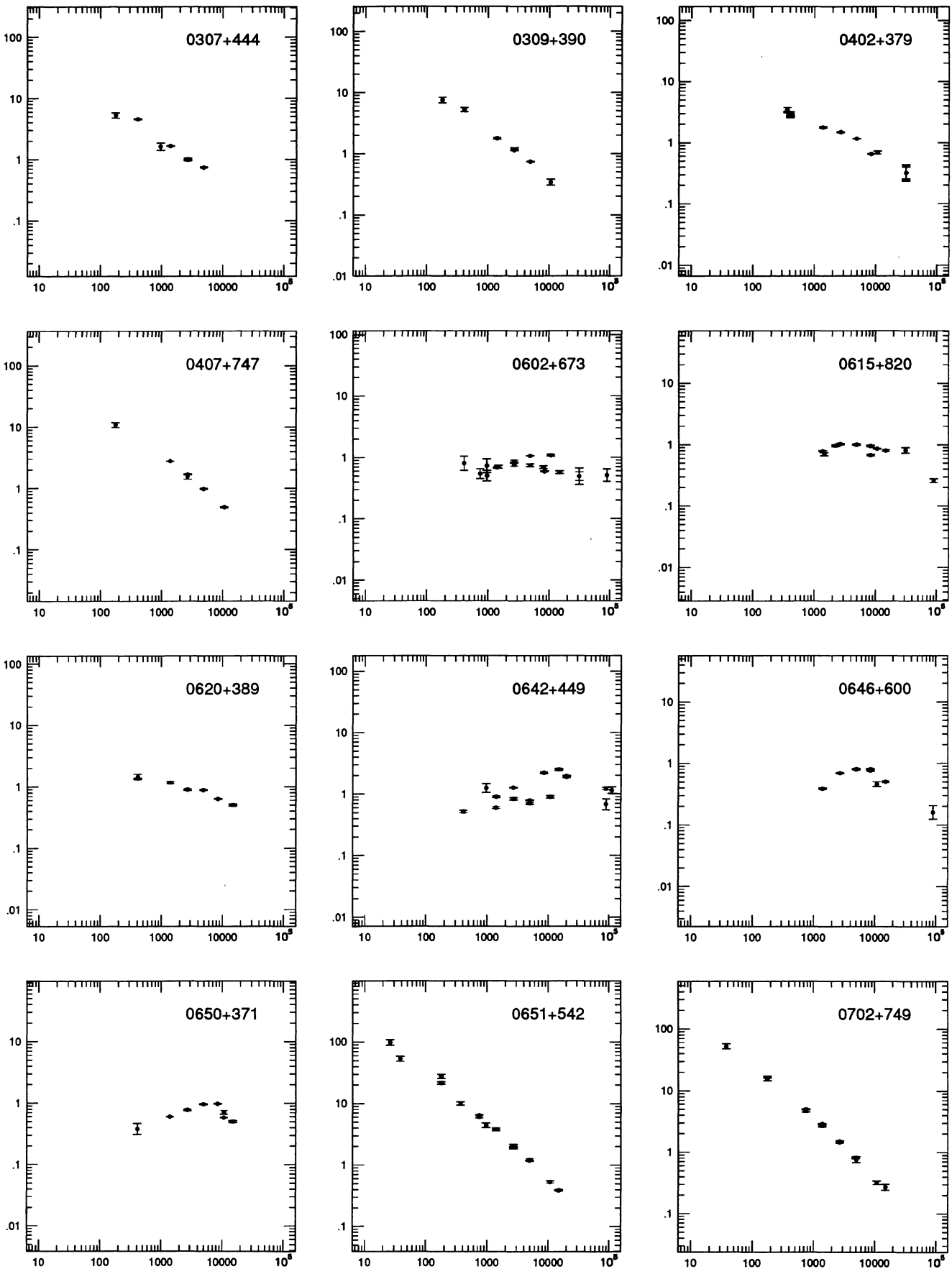

FIG. 7—*Continued*

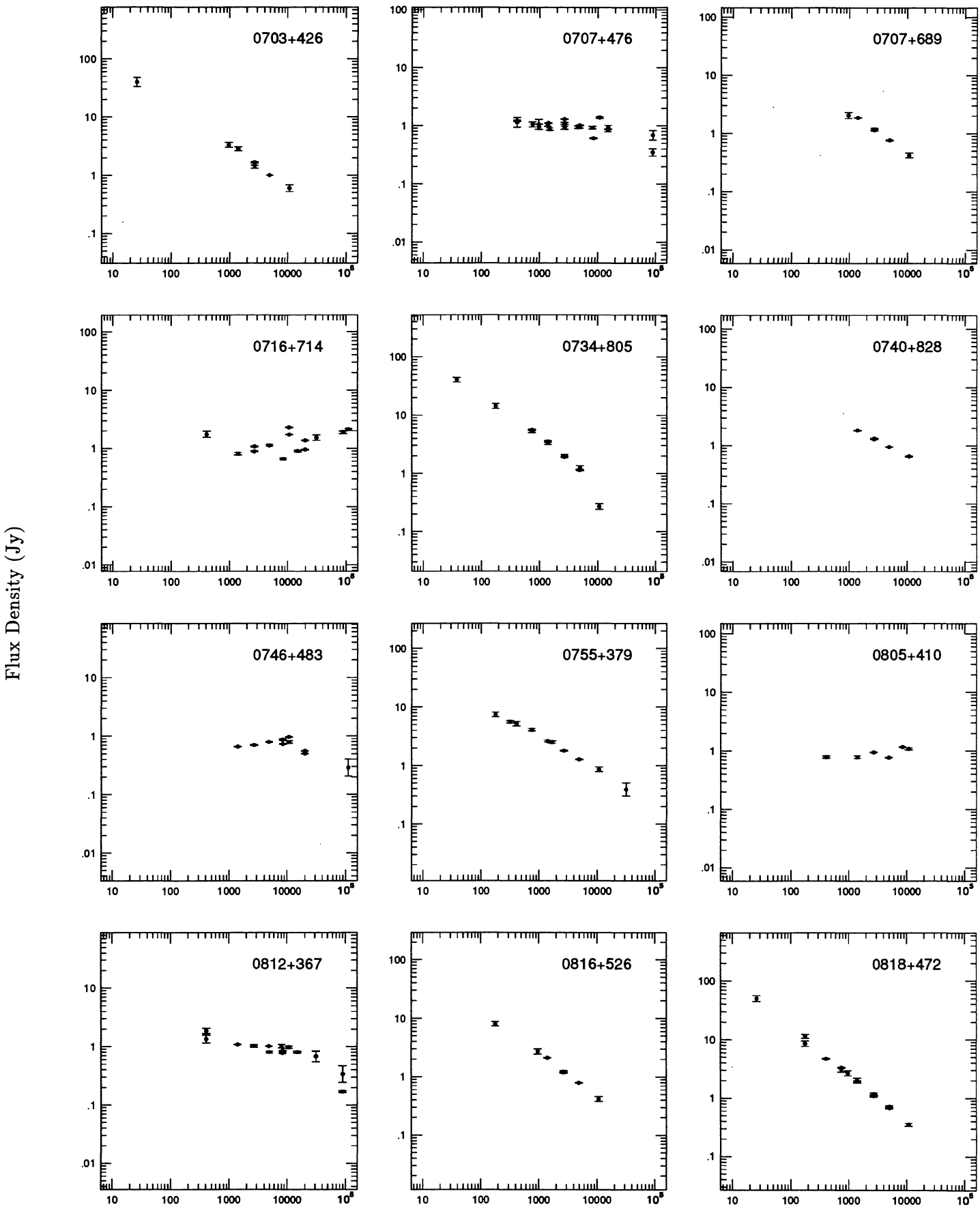

FIG. 7—*Continued*

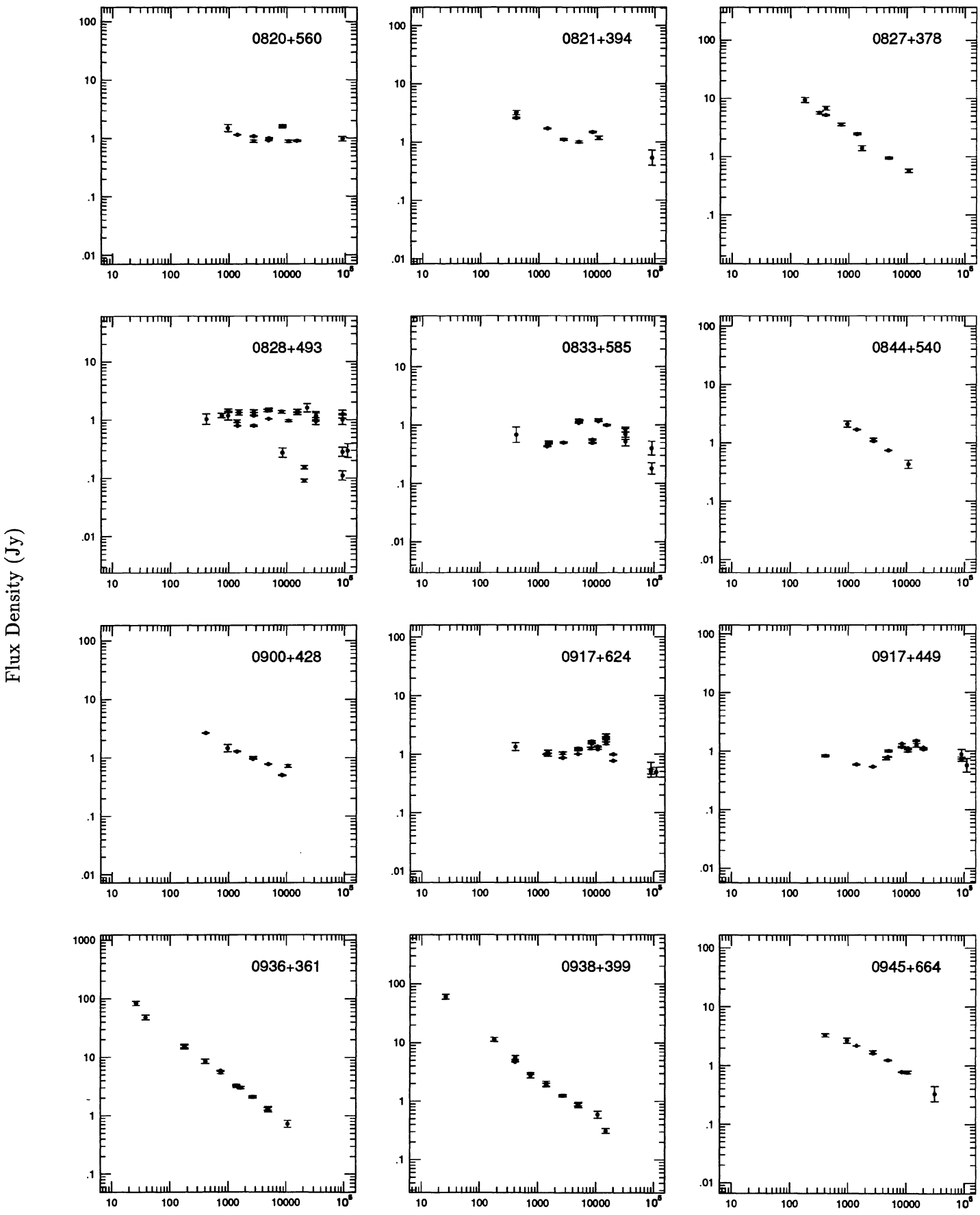

FIG. 7—*Continued*

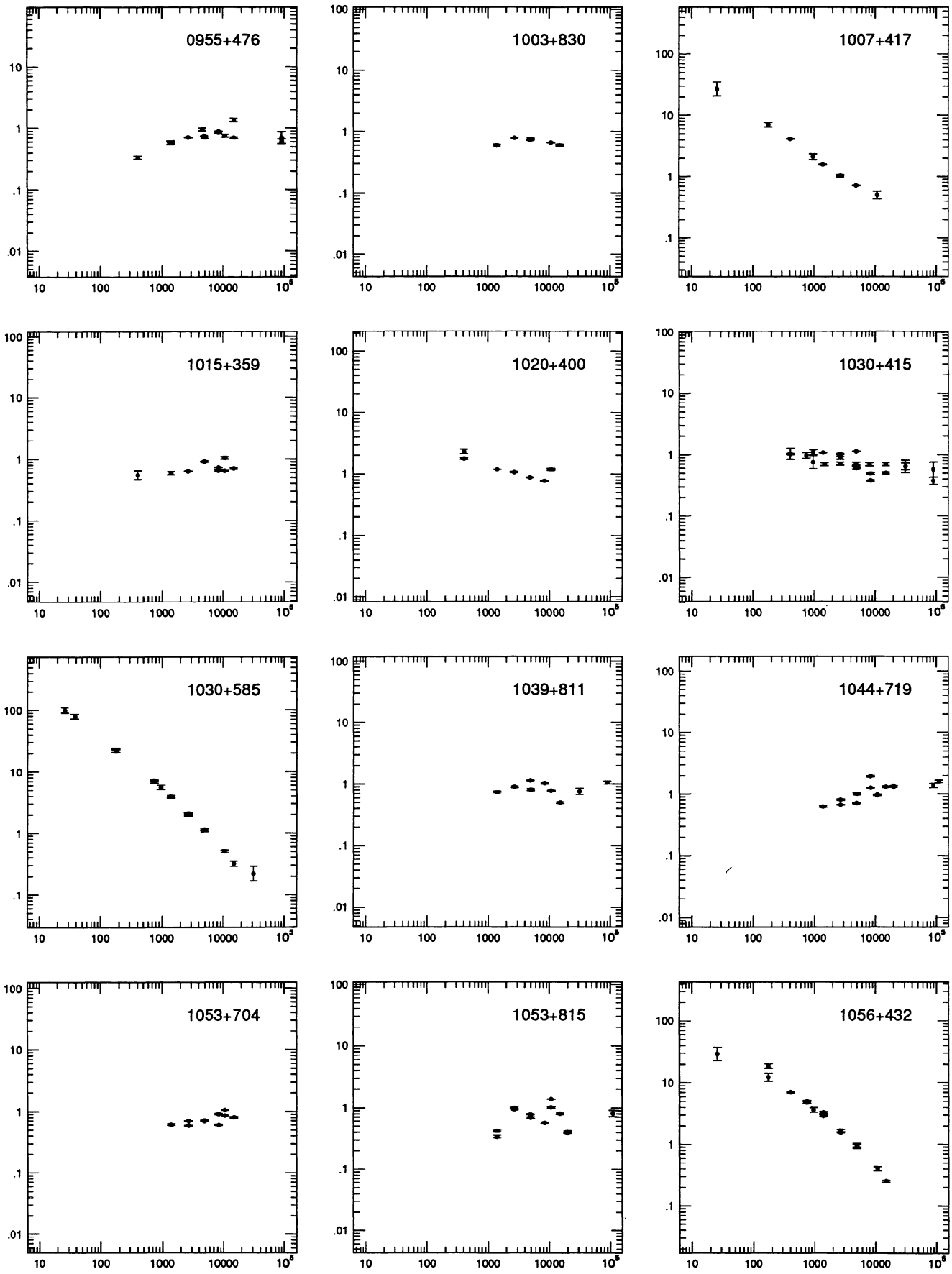

FIG. 7—*Continued*

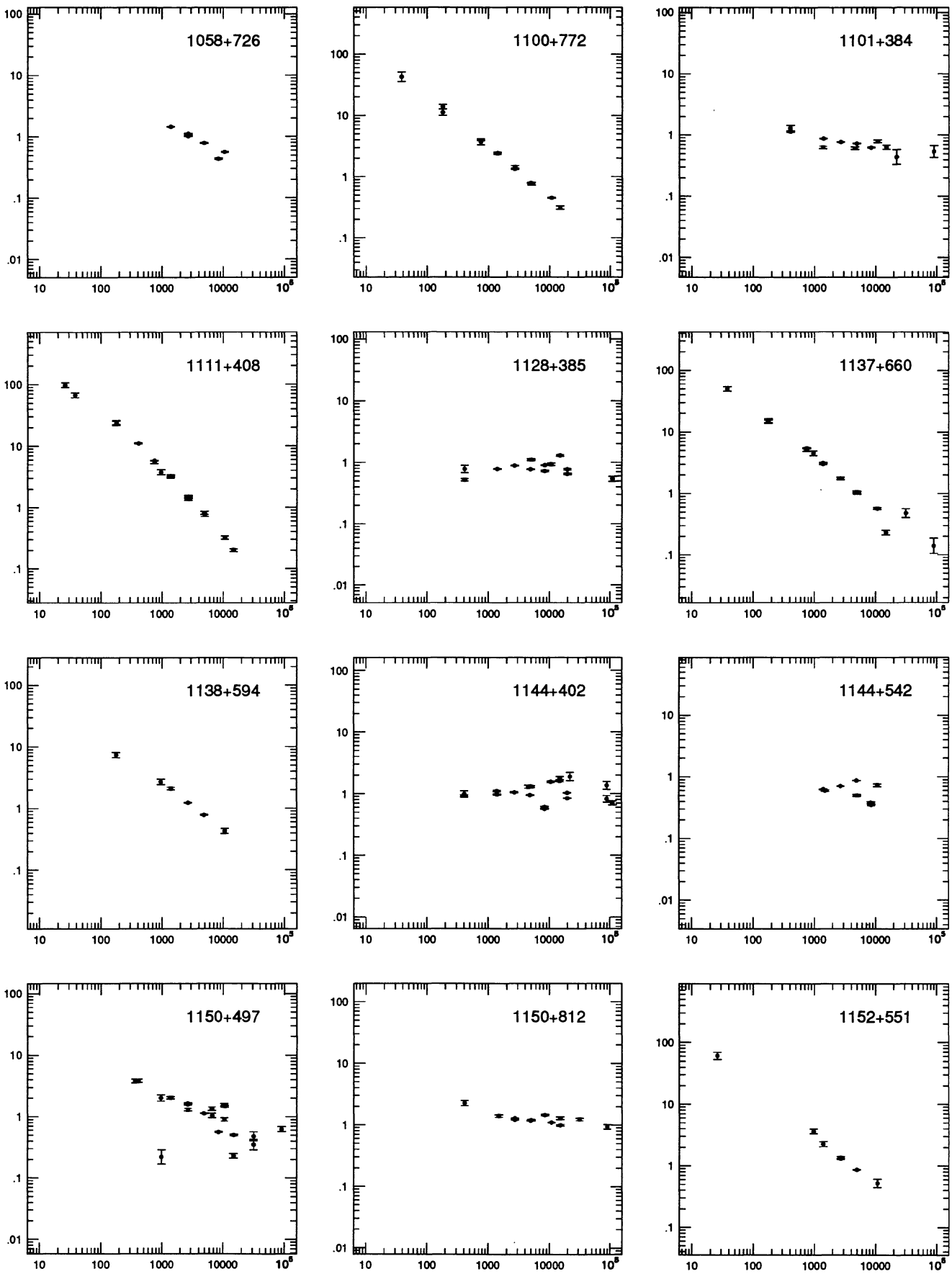

FIG. 7—*Continued*

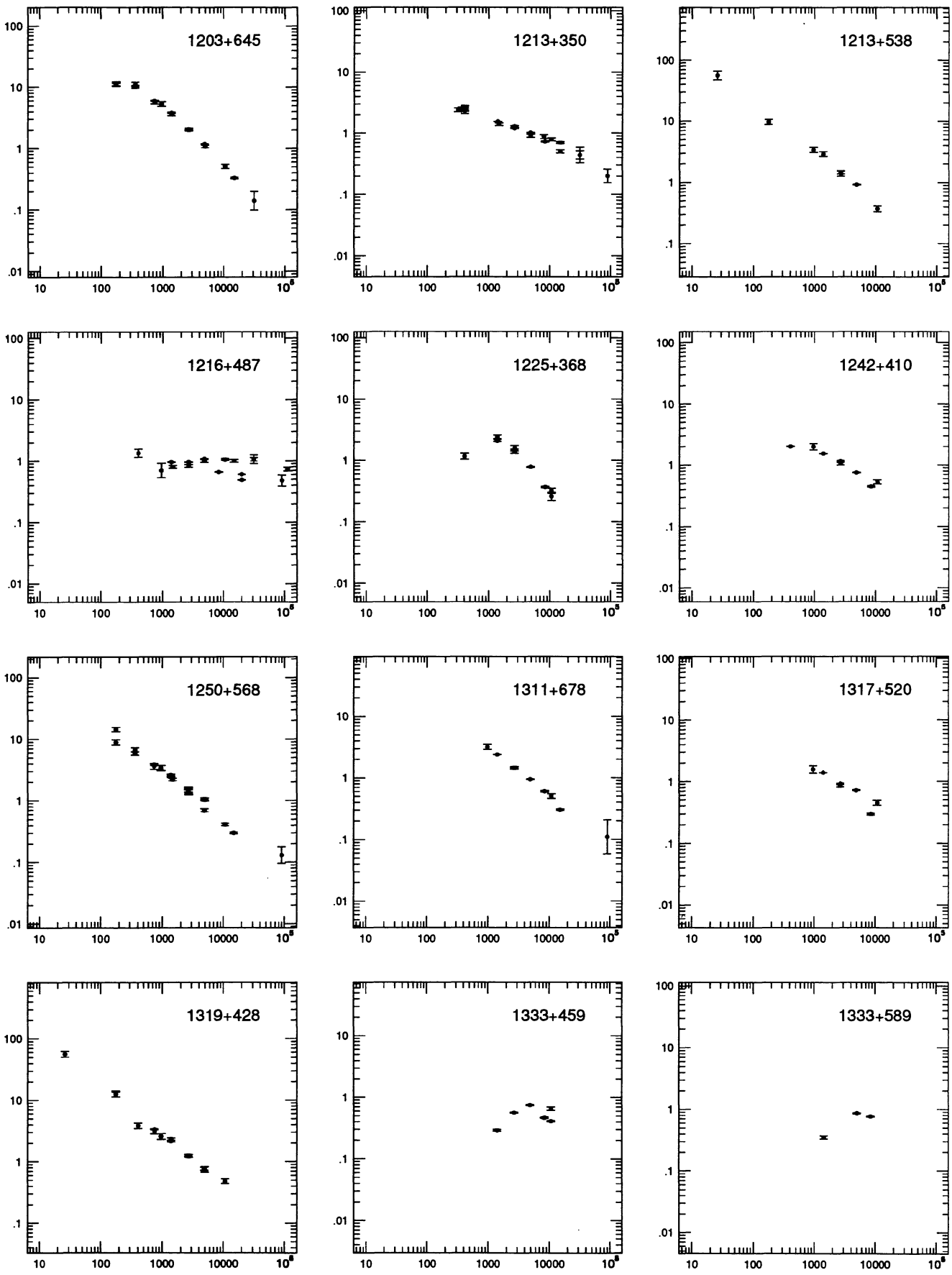

FIG. 7—*Continued*

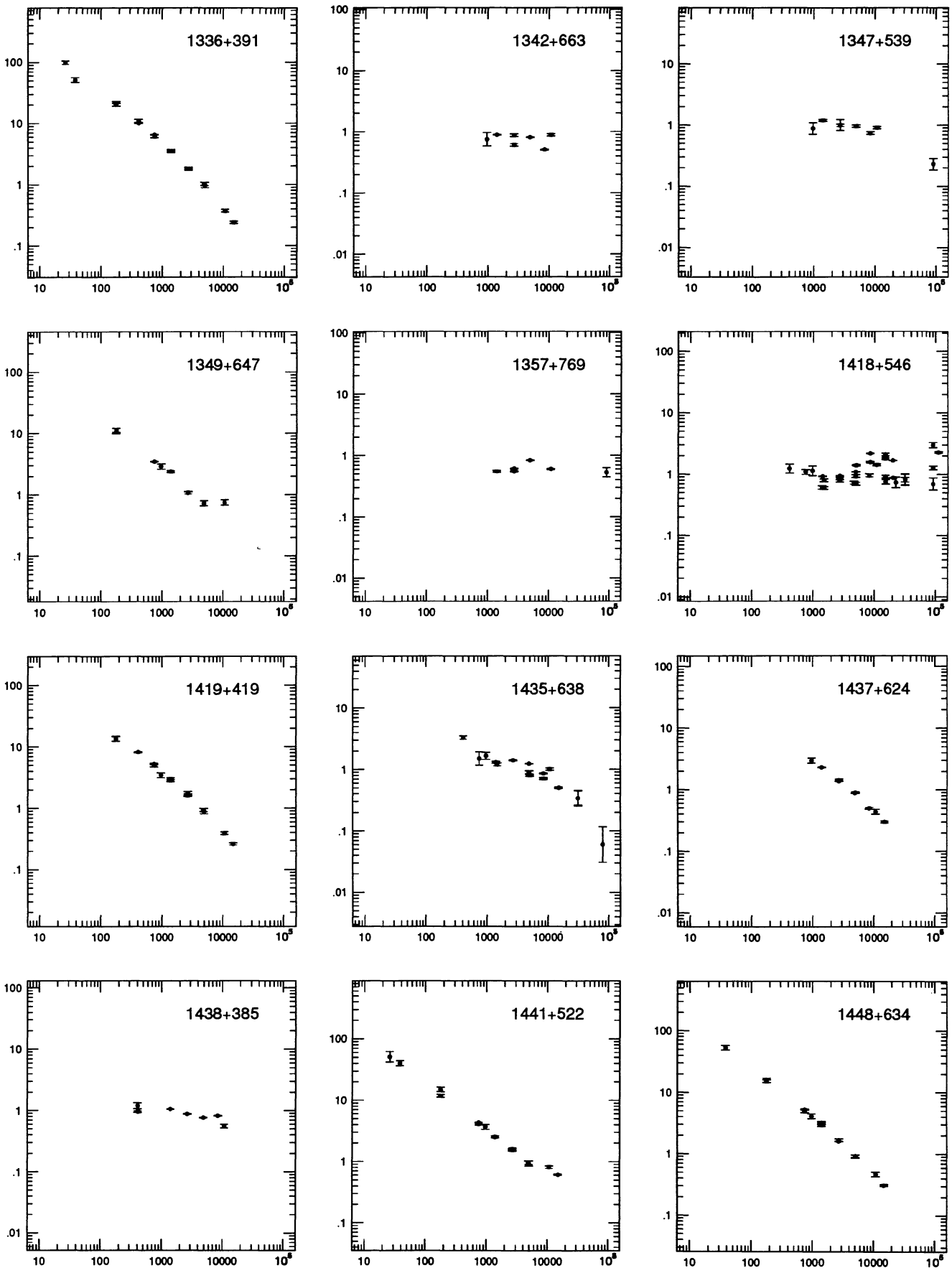

FIG. 7—*Continued*

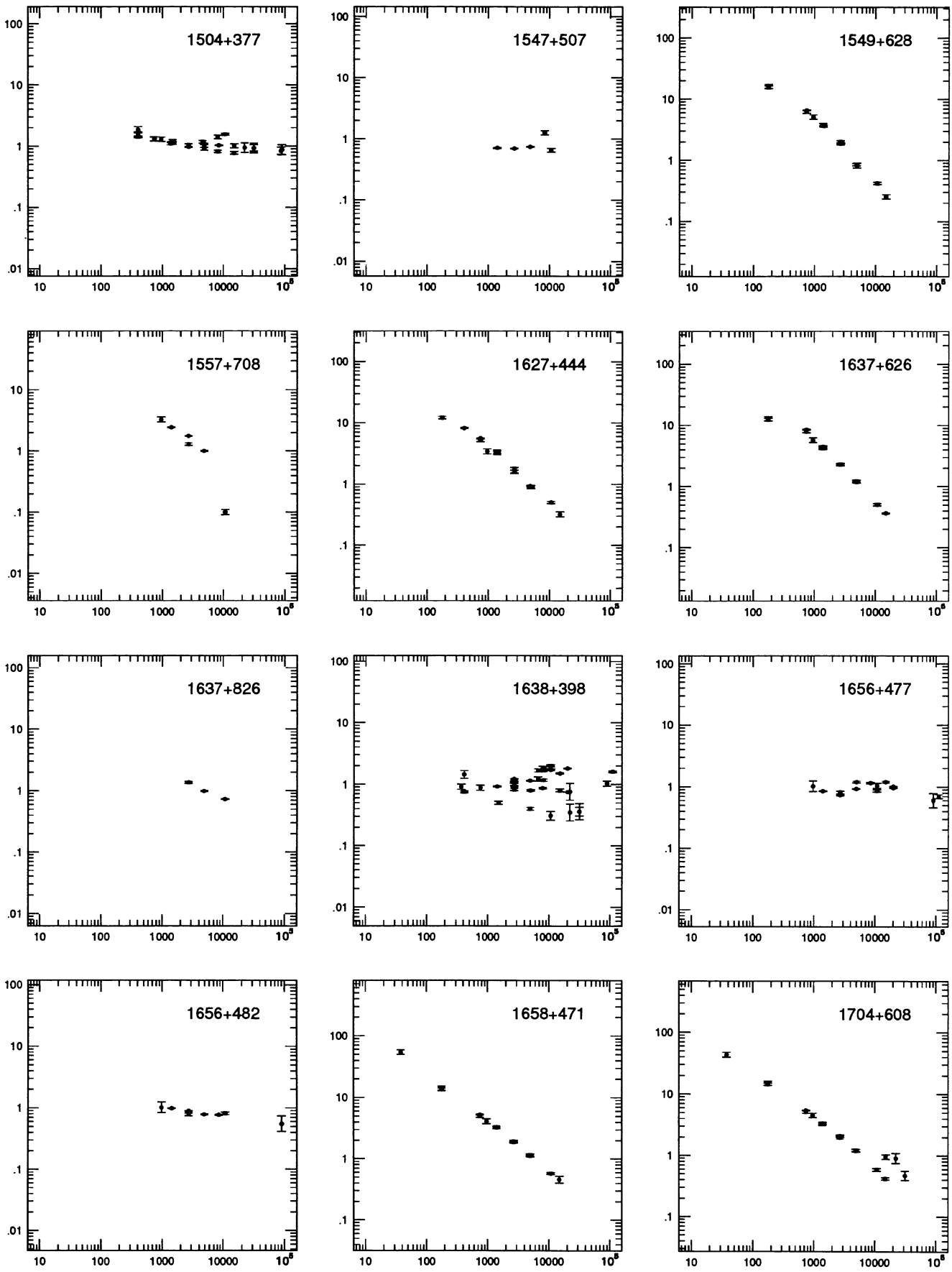

FIG. 7—*Continued*

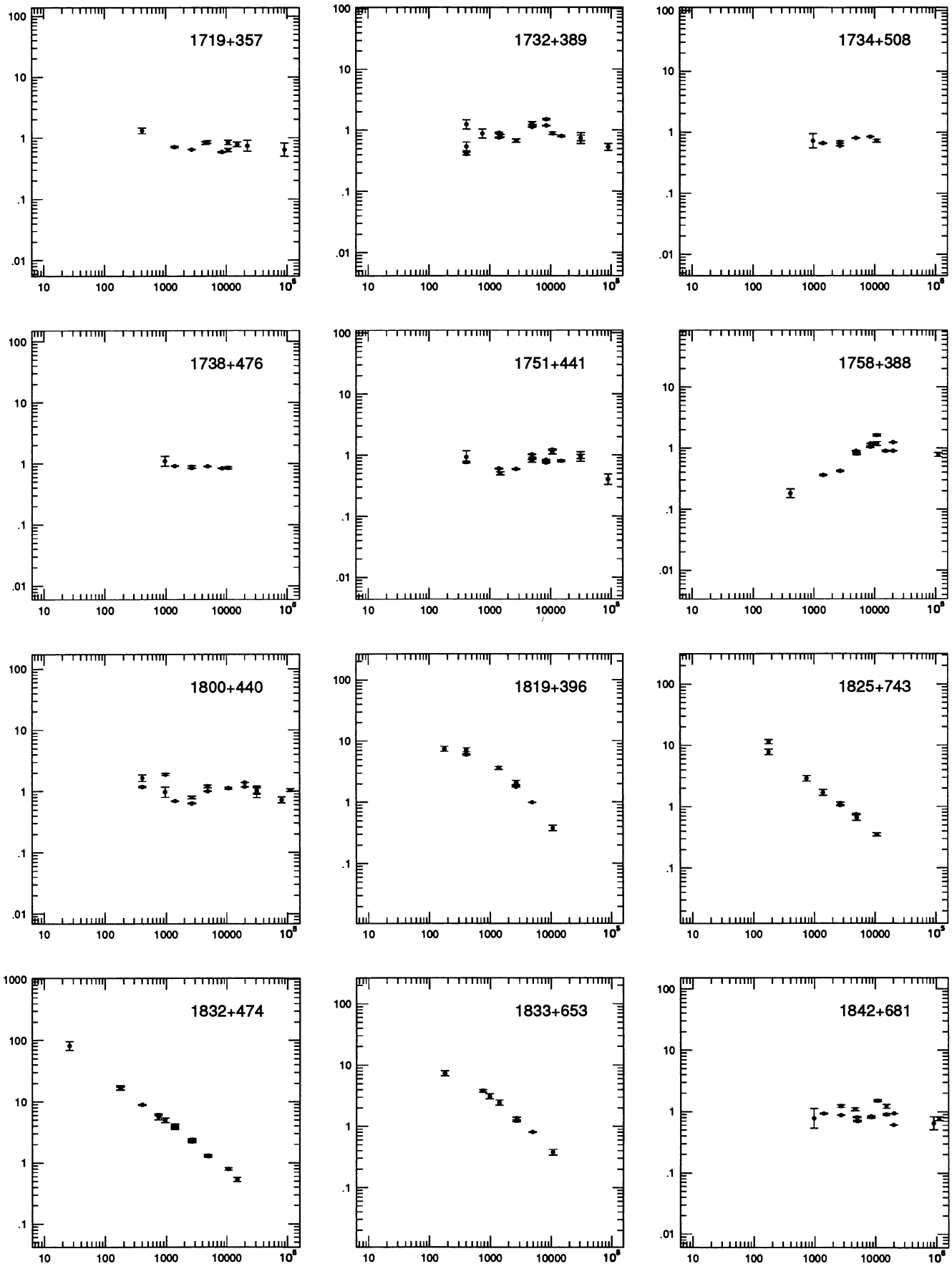

FIG. 7—*Continued*

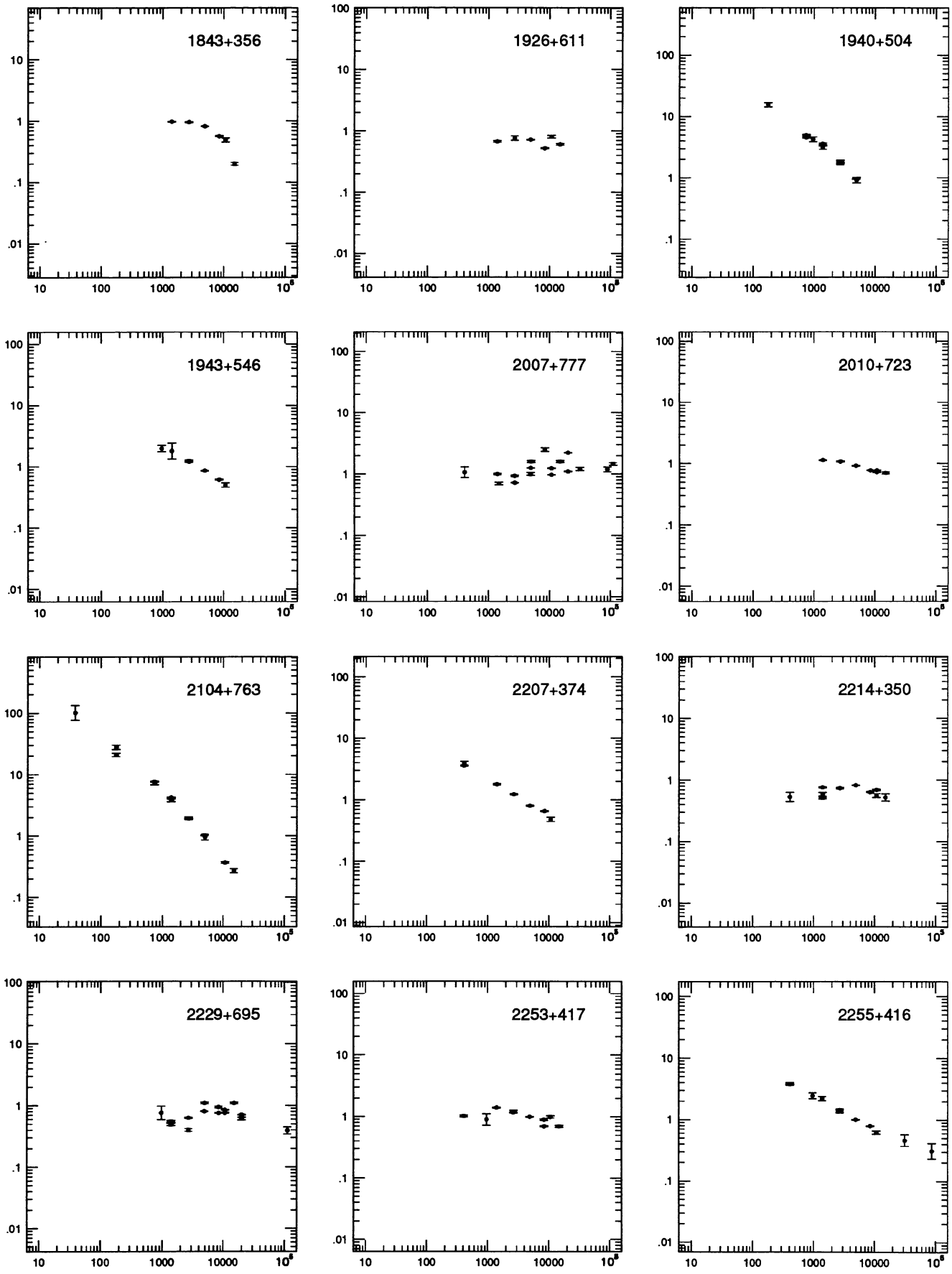

FIG. 7—*Continued*

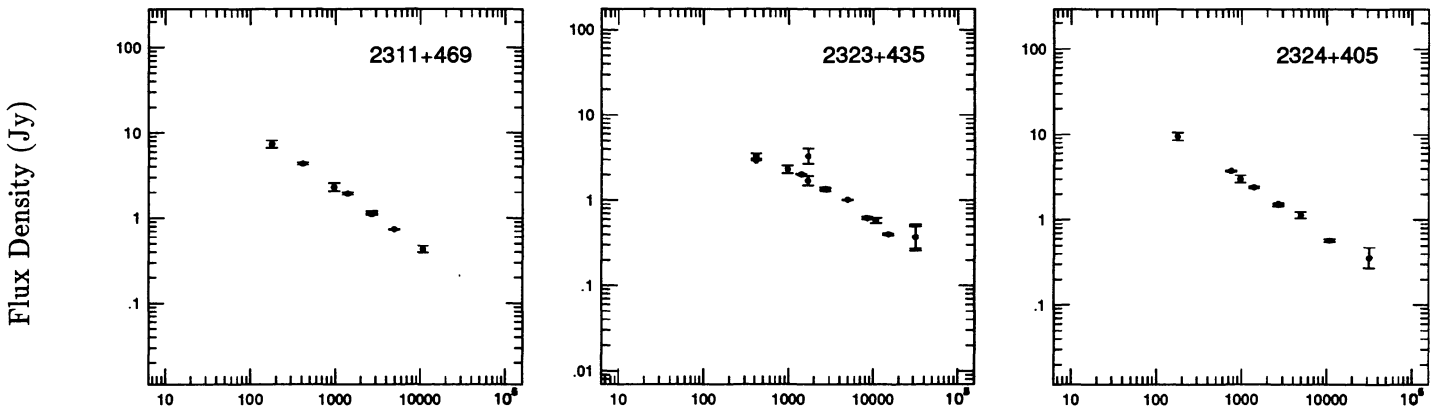

FIG. 7—*Continued*

2.3. *VLA Observations and Data Reduction*

Observations were made with the VLA in the A configuration at *L* band on 1992 November 5. Two IFs centered on 1464.9 and 1364.9 MHz, with a bandwidth of 50 MHz each, were used. The 92 objects observed are listed in Table 5. Each object was observed with three 2 minute snapshots, which were separated by 1.5 hr to improve the *uv* coverage. A typical *uv* coverage is shown in Figure 5. The data were reduced in the AIPS package. The object 3C 286 was used as the flux density calibrator. The MX program was used to make the maps and the CALIB program was used to perform self-calibration. In most cases the final maps were convolved with a circular Gaussian beam of FWHM 1".5. For objects dominated by large-scale structure, the final maps were convolved with a larger beam (3" or 5").

In VLA observations at this frequency there are often other radio sources present in the field. These objects must also be mapped in order to achieve high dynamic range on the target object. Thus we mapped an $11' \times 11'$ field for each object to locate possible confusing sources. All sources brighter than $\sim$10 mJy were mapped. The rms noise of a blank area of sky in the maps ranges from 0.1 to 0.5 mJy for most objects (see Table 5). Several strong sources have large rms noise, and this could not be corrected with self-calibration. Of the 92 objects, 28 are unresolved, and for these we do not present maps. The maps of the other 64 objects are presented in Figure 6, and the parameters of the maps are listed in Table 5.

2.4. *Radio Spectra*

The spectra of all the CJ1 objects are presented in Figure 7. We collected flux density measurements at various frequencies from the literature. For the most part, the data were taken from the catalog of radio objects compiled by Kühr et al. (1979). Part of the catalog containing objects brighter than 1 Jy has been published (Kühr et al. 1981b). Other data were taken from the VLA calibrator list (1990 edition); Edelson (1987); Ficarra, Grueff, & Tomassetti (1985); Patnaik et al. (1992); Steppe et al. (1988); and White & Becker (1992). Many of the sources are variable, and the flux density measurements span several years, so much of the apparent structure in the spectra can be attributed to variability.

3. CONCLUSION

In this third paper of the series, we have reported 5 GHz VLBI and MERLIN observations and 1.4 GHz VLA observations of objects in the CJ1 and PR samples. We now have a large body of observational data on the majority of objects in the complete sample of 200 objects with $S_{5\,\mathrm{GHz}} \geq 0.7$ Jy, $\delta \geq 35°$, and $|b| \geq 10°$, including VLBI images at 1.6 GHz (Papers I and II), VLBI images at 5 GHz (this paper and Pearson & Readhead 1988), MERLIN and VLA images (this paper and published results), and radio spectra (this paper). Optical observations to measure redshifts are in progress (Xu et al. 1994).

The CJ1+PR sample of 200 objects is large enough to refine the classification of compact radio objects presented by Pearson & Readhead and to undertake a number of important astrophysical and cosmological studies. These subjects will be addressed in subsequent papers in the series. A number of particularly interesting objects have already been identified, including several compact symmetric objects (e.g., 2352+495: Wilkinson et al. 1994; Readhead et al. 1995), gravitational lenses (e.g., 0218+357; Patnaik et al. 1993), and a high-redshift superluminal object (0642+449: Vermeulen et al. 1995).

While this paper completes the VLBI observations for the CJ1 survey, we are also in the process of enlarging the sample still further with the second Caltech–Jodrell Bank VLBI survey (CJ2) of flat-spectrum radio objects (Taylor et al. 1994; Henstock et al. 1995).

We thank the staffs of the observatories in the European and the US VLBI networks and the staff of the JPL/Caltech Block 2 correlator for their assistance during the CJ1 survey. We also thank R. C. Vermeulen and G. B. Taylor for their help with

fringe-fitting and automatic mapping and G. B. Taylor and D. R. Henstock for observing six objects for us. A. G. P. acknowledges the receipt of a British Council Fellowship for the year 1991. The work at the California Institute of Technology was supported by the National Science Foundation (grants AST-8814554 and AST-9117100). The VLA and VLBA are instruments of the National Radio Astronomy Observatory, which is operated by Associated Universities, Inc., under cooperative agreement with the National Science Foundation.

REFERENCES

Clark, B. G. 1973, Proc. IEEE, 61, 1242
Cohen, M. H., et al. 1975, ApJ, 201, 249
Edelson, R. A. 1987, AJ, 94, 1150
Ficarra, A., Grueff, G., & Tomassetti, G. 1985, A&AS, 59, 255
Henstock, D. R., Wilkinson, P. N., Browne, I. W. A., Taylor, G. B., Vermeulen, R. C., Pearson, T. J., & Readhead, A. C. S. 1995, ApJS, in press
Högbom, J. A. 1974, A&AS, 15, 417
Jones, D. L., et al. 1986, ApJ, 305, 684
Kühr, H., Nauber, U., Pauliny-Toth, I. I. K., & Witzel, A. 1979, MPIfR preprint 55
Kühr, H., Pauliny-Toth, I. I. K., Witzel, A., & Schmidt, J. 1981a, AJ, 86, 854
Kühr, H., Witzel, A., Pauliny-Toth, I. I. K., & Nauber, U. 1981b, A&AS, 45, 367
Patnaik, A. R., Browne, I. W. A., King, L. J., Muxlow, T. W. B., Walsh, D., & Wilkinson, P. N. 1993, MNRAS, 261, 435
Patnaik, A. R., Browne, I. W. A., Wilkinson, P. N., & Wrobel, J. M. 1992, MNRAS, 254, 655
Pauliny-Toth, I. I. K., Witzel, A., Preuss, E., Kühr, H., Kellermann, K. I., Fomalont, E. B., & Davis, M. M. 1978, AJ, 83, 451
Pearson, T. J. 1991, BAAS, 23, 991
Pearson, T. J., & Readhead, A. C. S. 1988, ApJ, 328, 114 (PR)
Polatidis, A. G., Wilkinson, P. N., Xu, W., Readhead, A. C. S., Pearson, T. J., Taylor, G. B., & Vermeulen, R. C. 1995, ApJS, 98, 1 (Paper I)
Readhead, A. C. S., Xu, W., Pearson, T. J., Taylor, G. B., Wilkinson, P. N., & Polatidis, A. G. 1995, in preparation
Schwab, F. R., & Cotton, W. D. 1983, AJ, 88, 688
Shepherd, M. C., Pearson, T. J., & Taylor, G. B. 1994, BAAS, 26, 987
Steppe, H., Salter, C. J., Chini, R., Kreysa, E., Brunswig, W., & Lobato Perez, J. 1988, A&AS, 75, 317
Taylor, G. B., Vermeulen, R. C., Pearson, T. J., Readhead, A. C. S., Henstock, D. R., Browne, I. W. A., & Wilkinson, P. N. 1994, ApJS, 95, 345
Thakkar, D. D., Xu, W., Readhead, A. C. S., Pearson, T. J., Taylor, G. B., Vermeulen, R. C., Polatidis, A. G., & Wilkinson, P. N. 1995, ApJS, 98, 33 (Paper II)
White, R. L., & Becker, R. H. 1992, ApJS, 79, 331
Wilkinson, P. N., Polatidis, A. G., Readhead, A. C. S., Xu, W., & Pearson, T. J. 1994, ApJ, 432, L87
Xu, W., Lawrence, C. R., Readhead, A. C. S., & Pearson, T. J. 1994, AJ, 108, 395
Vermeulen, R. C., et al. 1995, in preparation